An alternative AUG codon in segment 5 of the 2009 pandemic influenza A virus is a swine-derived virulence motif

Helen M. Wise[1,2*], Eleanor Gaunt[1*], Jihui Ping[3], Barbara Holzer[4], Seema Jasim[1], Samantha J. Lycett[1], Lita Murphy[1], Alana Livesey[2], Russell Brown[2], Nikki Smith[1], Sophie Morgan[4], Becky Clark[4], Katerine Kudryavtseva[2], Philippa M. Beard[1,4], Jonathan Nguyen-Van-Tam[5], Francisco J. Salguero[6], Elma Tchilian[4], Bernadette M. Dutia[1], Earl G. Brown[3] and Paul Digard[1]

[1]The Roslin Institute, University of Edinburgh, Easter Bush, Midlothian EH25 9RG, UK.
[2]Division of Virology, Department of Pathology, University of Cambridge, Tennis Court Road, Cambridge CB2 1QP, UK.
[3]Department of Biochemistry, Microbiology and Immunology, University of Ottawa, Canada.
[4]The Pirbright Institute, Ash Road, Pirbright, Woking, Surrey GU24 0NF, UK.
[5]Division of Epidemiology and Public Health, University of Nottingham School of Medicine, Clinical Sciences Building, City Hospital Campus, Hucknall Road, Nottingham NG5 1PB, UK.
[6] Public Health England, PHE Porton, Manor Farm Road, Porton Down, Salisbury SP4 0JG, UK.
[*]Equal contributions.

Current addresses:
HMW: Clinical biochemistry, Clock Tower building, Western General Hospital, Edinburgh, EH4 2XU, UK
JP: Institute of Immunology, College of Veterinary Medicine, Nanjing Agricultural University, China
SJ: MRC-University of Glasgow Centre for Virus Research, Glasgow, G61 1QH, UK
SM: Respiratory Medicine Unit, NDM Experimental Medicine, University of Oxford, John Radcliffe Hospital, Oxford, OX3 9DU, UK

Corresponding author: Paul Digard, paul.digard@roslin.ed.ac.uk

Abstract

The 2009 influenza A virus (IAV) pandemic (pdm2009) was caused by a swine H1N1 virus with several atypical genetic features. Here, we investigate the origin and significance of an upstream AUG (uAUG) codon in the 5'-untranslated region of the NP gene. Phylogeny indicated that the uAUG codon arose in the classical swine IAV lineage in the mid 20th Century, and has become fixed in the current triple reassortant, variant pdm2009 swine IAV and human pdm2009 lineages. Functionally, it supports leaky ribosomal initiation *in vitro* and *in vivo* to produce two isoforms of NP: canonical, and a longer "eNP". The uAUG codon had little effect on viral gene expression or replication *in vitro*. However, in both murine and porcine models of IAV infection, removing the uAUG codon gene attenuated pdm2009 virus pathogenicity. Thus, the NP uAUG codon is a virulence factor for swine IAVs with proven zoonotic ability.

Introduction

The 2009 influenza A virus (IAV) pandemic was caused by a swine-origin H1N1 (pdm2009) virus that, although highly transmissible, was markedly less pathogenic and caused substantially lower mortality than 20th Century pandemic strains. Notwithstanding marked regional variation in the incidence of severe disease, estimates place the overall human mortality burden from the pandemic phase of pdm2009 at a similar level to disease caused by the preceding seasonal strains (1,2). Initial sequencing of the pdm2009 virus highlighted several features that could potentially explain this unexpectedly mild pathogenicity phenotype (3). These included a PB2 subunit of the viral RNA polymerase with avian-signature motifs at positions 627 and 701, a disrupted PB1-F2 gene, polymorphisms in the NS1 protein that abrogated host cell translational shut-off activity and removed a PDZ-binding domain, as well as a truncated PA-X gene (3-6). A further unusual feature of the pdm2009 genome is the presence of an upstream AUG (uAUG) codon in the 5' untranslated region (UTR) of segment 5 (7). Segment 5 encodes the viral nucleoprotein (NP); a single strand RNA-binding protein that (along with the viral polymerase) encapsidates the single-stranded IAV genomic RNA segments into ribonucleoprotein (RNP) particles and thereby plays an essential role in supporting viral RNA synthesis (8,9). NP also contains nuclear localisation (NLS) and nuclear export signals and, in concert with the viral matrix (M1) and nuclear export protein (NEP) as well as many cellular proteins, helps direct the nuclear import of the viral genome at the start of infection and its export after genome replication (9). This functional importance is reflected in a high level of sequence conservation across IAV strains (10) and unlike the viral HA, NA and NS1 proteins, length polymorphisms of NP are very rare. However, the NP uAUG codon is in frame with the main NP open reading frame (ORF) and, if used for translation initiation, would add an extra 6 amino-acids to the N-terminus of the protein. The N-terminal 20 amino acids of NP form a

flexible region not visible in crystal structures of the polypeptide (11,12) and contain the primary NLS of the polypeptide responsible for nuclear import of monomeric NP and RNPs (13-15). It was therefore reasonable to hypothesise that an alteration to this region to produce an extended NP (eNP) variant would have functional consequences for the protein that could downregulate viral pathogenicity, thus providing an explanation for the unexpectedly low levels of morbidity seen during the 2009 pandemic. Here, we describe a test of this hypothesis that shows that while eNP is produced in infection and the uAUG codon does affect *in vivo* viral pathogenicity in mice and pigs, it unexpectedly acts to increase virulence.

Results

The NP uAUG codon is of swine IAV origin

Segment 5 of the pdm2009 virus was acquired from the H1N1 classical swine virus lineage which in turn is a descendant of the 1918 pandemic strain, which lacked the uAUG (16,17). Examination of all available IAV segment 5 sequences on the Genbank database that reported the 5'-UTR indicated that possession of the uAUG is a minority trait, with 9104 of 33622 sequenced viruses (27%) containing it. However, within this overall population, there were clear differences between viruses from different host species (Fig 1A, Table 1), with the uAUG being extremely rare in avian isolates (~ 0.3%) but very frequent (approaching 90%)

Table 1. Prevalence of the uAUG in IAV segment 5 sequences

Host	Number of sequences	Conventional Start	uAUG start (%)
Avian	11210	11176	34 (0.3)
Swine	2396	261	2135 (89.1)
Human	19772	12852	6920 (35.0)
Other	244	229	15 (6.1)
Total	33622	24518	9104 (27.1)

in swine viruses. Around one third of human isolates contain the segment 5 uAUG, with the vast majority of these being pdm2009 isolates.

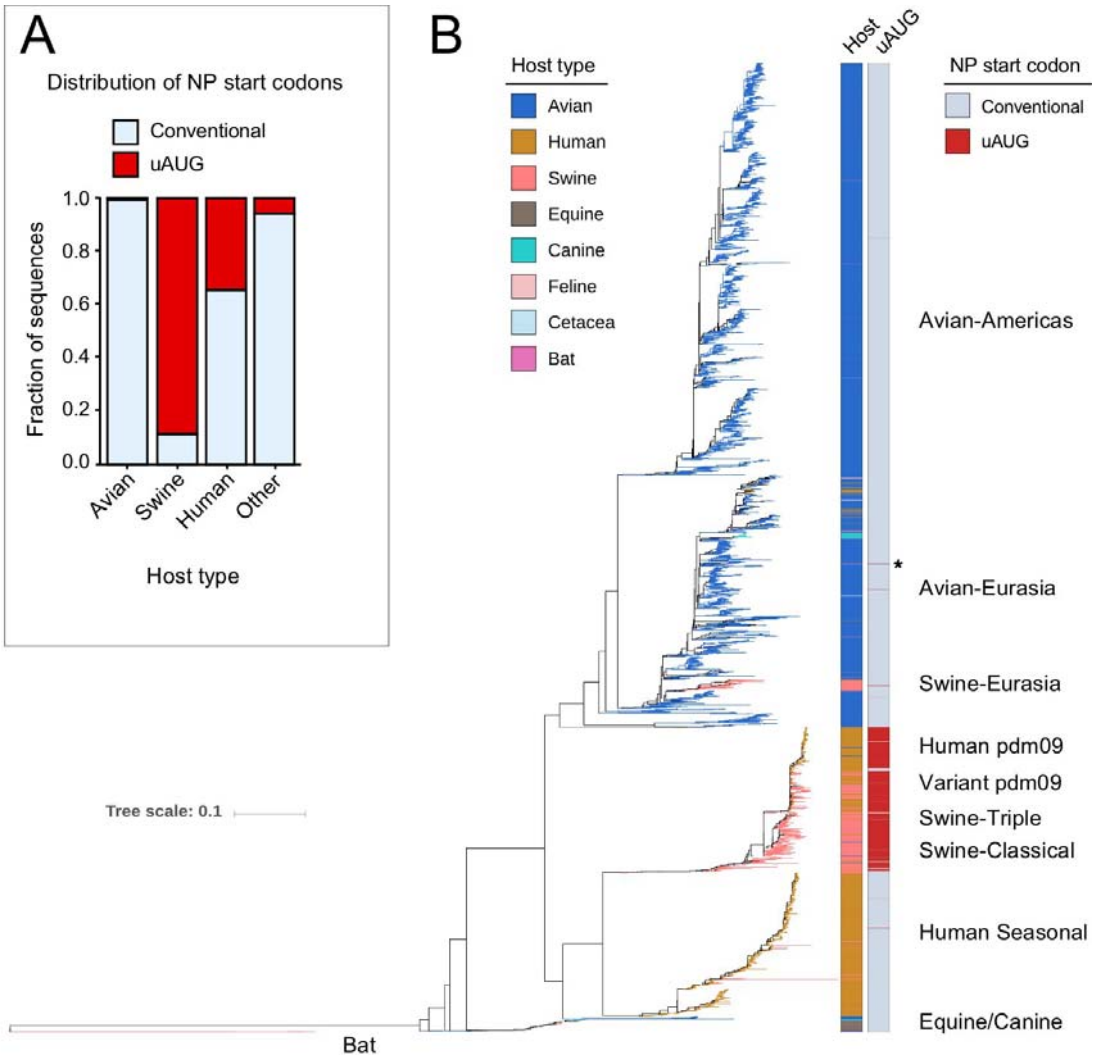

Figure 1. Phylogenetic analysis of segment 5 uAUG occurrence. (A) The fraction of segment 5 sequences that report the 5'-UTR, split into broad host categories, that contain the uAUG codon (red) or only the conventional NP start codon (blue). (B) Maximum likelihood phylogenetic tree of stratified subsampled sequences. Tips and left hand bar are coloured according to host while the right hand bar reports the presence (red) or absence (blue) of the uAUG start codon. Major lineages are indicated. The section of the tree indicated with an asterisk is reported in greater detail in Figure S4.

106 To examine the evolution of the uAUG in IAV, a phylogenetic tree for segment 5 was
107 constructed from a stratified subsampled dataset of over 6000 sequences (Tables S1, S2) and
108 coloured according to host species and the presence or absence of the uAUG (Fig 1B). This
109 indicated that the uAUG is primarily a feature of the classical swine virus segment 5 and, by
110 descent (18), the triple reassortant, pdm2009 and variant pandemic lineages (Table S1, Table
111 S2, Fig S1). Within this clade, the uAUG codon evolved in the early 1960s in the US swine
112 population, becoming predominant by the 1970s (Fig S2). The uAUG polymorphism also
113 shows almost complete fixation in the subsequent triple reassortant, pdm2009 and variant
114 swine virus lineages (93% of the sequences analysed; Fig S3, Table S1). In addition, the
115 uAUG appears to have arisen independently on several other occasions: two or three times
116 each in the avian and human seasonal H3N2 lineages, detectably persisting for no more than
117 two or three years at most (Table S3), as well as twice within swine IAVs. One of the swine
118 episodes reflects a relatively short-lived occurrence, in which an H5N1 virus transferred from
119 ducks to pigs (19), gaining the uAUG codon around the time of the epizootic transition (Fig
120 S4). The other occasion represents a localized gain of the uAUG within the Eurasian swine
121 IAV lineage in Hong Kong in the early/mid 2000s (Fig S5). Thus overall, segment 5 has
122 gained the uAUG codon on at least seven occasions; three of these were associated with
123 swine IAV and the first of these, acquired in the background of a segment from the 1918
124 pandemic virus, has persisted for over half a century and resulted in world-wide colonization
125 of swine, and via the 2009 pandemic, man.
126
127 **Initiation of translation occurs from the segment 5 uAUG in cell-free and cell-based**
128 **systems**
129 The phylogenetic data suggested the hypothesis that the uAUG provided a host-
130 specific selective advantage in H1N1 viruses. As a first test of its biological significance, we

asked if it was used for translation. The uAUG arises from a C28A polymorphism and is in frame with the canonical start codon of the NP ORF (AUG1) such that, if used, it would

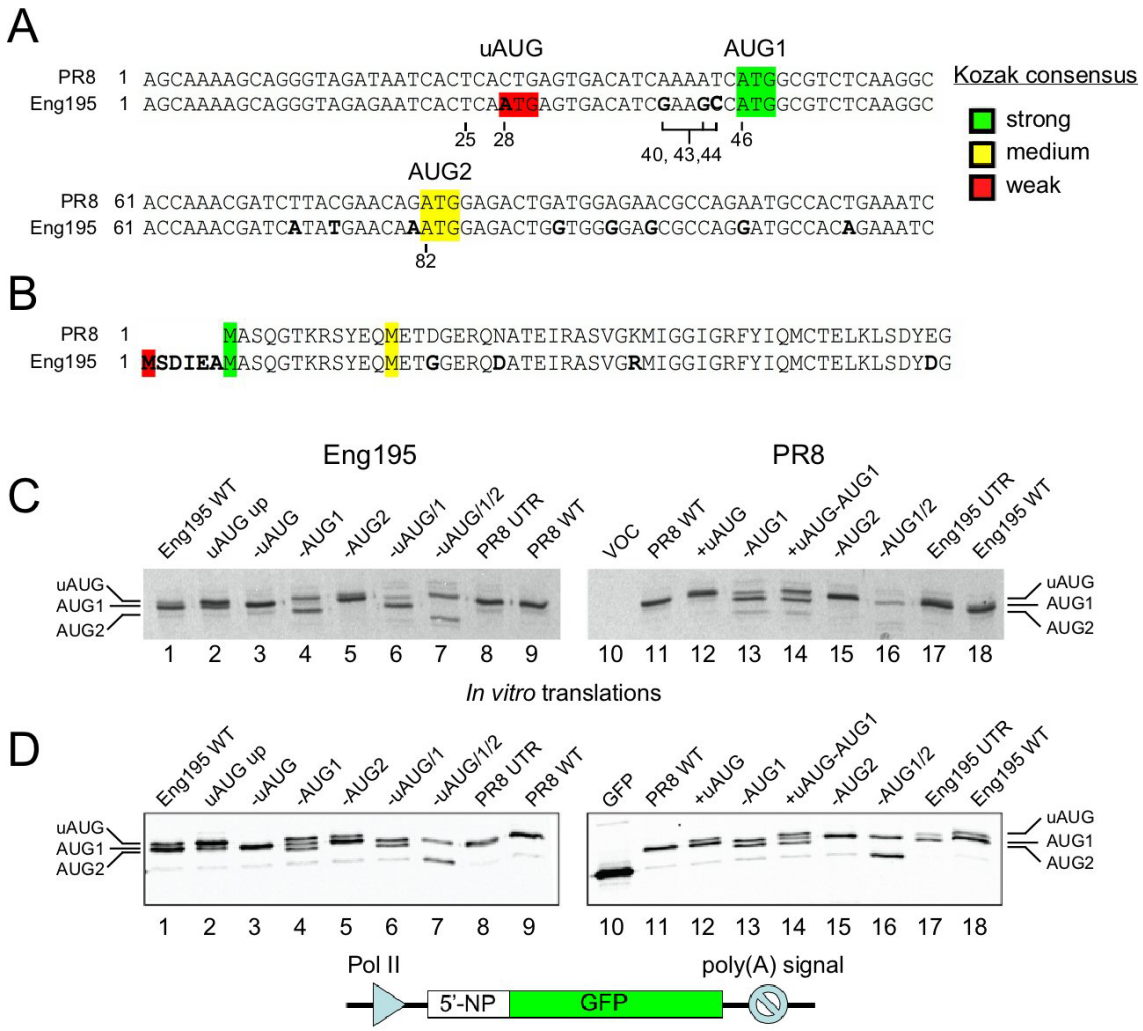

Figure 2. Sequence and translation initiation potential of IAV segment 5. (A) Nucleotide sequence of the 5'-end (mRNA sense, starting from position 1 of cRNA; *i.e.* ignoring any cap-snatched leader sequence) of segment 5 from PR8 and Eng195 strains. Differences are highlighted in bold, while AUG codons are colour-coded according to their Kozak initiation potential. Numbered positions were targeted for mutagenesis. (B) Amino-acid sequence of the N-terminal region of NP, highlighted as above. (C) Aliquots of rabbit reticulocyte lysate coupled *in vitro* transcription/translation reactions supplemented with ^{35}S-methionine were programmed with pDUAL plasmids containing cDNA copies of the indicated WT and mutant segment 5s (or empty vector; VOC) before separation by SDS-PAGE. Radiolabelled translation products were detected by autoradiography. (D) Lysates from 293T cells transfected with plasmids containing the 5'-201 nucleotides of segment 5 cDNA, either WT or mutated as labelled, fused in frame with GFP (or with a plasmid only encoding GFP) were separated by SDS-PAGE and western blotted for NP. The migration position of polypeptides starting at the first three AUG codons is indicated.

produce an extended NP polypeptide with a 6 amino-acid extension (Figs 2A, B). However, the uAUG codon is in a poor 'Kozak' context for translation initiation (20) so it was unclear if, or to what extent, it might be seen by scanning ribosomes and used for translation initiation. A similarly poor context AUG codon near the 5'-end of segment 2 of IAV is not seen by scanning ribosomes to any appreciable extent (21). To address whether the segment 5 uAUG is used for translation, we created a series of constructs based on segment 5 cDNA, from either the UK prototype pdm2009 virus A/England/195/2009 (Eng195) (22) or the laboratory-adapted A/Puerto Rico/8/34 (PR8) H1N1 strain, with mutations designed to alter potential translation start sites in the first 100 nucleotides. These included removing the uAUG from Eng195 or adding it to PR8 by A28C/C28A switches, altering AUGs 1 and 2 to CUG codons, improving the Kozak consensus sequence of uAUG (by U25G) and reciprocally swapping the context of AUG1 (by mutating nucleotides 40, 43 and 44) between Eng195 and PR8 identities (Fig 2A).

These plasmids were then used to programme radiolabelled coupled *in vitro* transcription-translation reactions in rabbit reticulocyte lysate and polypeptide synthesis was monitored by SDS-PAGE (run for longer than normal to separate polypeptides predicted to differ in molecular weight by < 1 kDa) and autoradiography. The wild type (WT) PR8 plasmid directed synthesis of a single major polypeptide species whereas WT Eng195 gave a doublet in which the slower migrating species was less abundant (Fig 2C, compare lane 1 with 9, and lane 11 with 18), consistent with translation initiation at either of two closely spaced AUG codons in the Eng195 segment 5 mRNA. Further supporting this conclusion, improving the Kozak consensus of the Eng195 uAUG altered the proportions of the doublet so that the upper band was predominant, while mutating the uAUG removed it (Fig 2C, lanes 2 and 3). Confirming the likely identity of the polypeptides, mutation of AUG1 to CUG further changed the ratio of the doublet species, with only a trace of the smaller polypeptide

now visible, but with the addition of a more prominent faster migrating band (lane 4) that co-migrated with trace species visible in WT and other AUG1-containing translation reactions. Mutation of AUG2 removed this fast-migrating product (lane 5), suggesting that leaky ribosomal scanning past an inefficiently recognised uAUG in the absence of AUG1 led to increased usage of AUG2 for translation initiation. The small amount of a polypeptide with the expected size for canonical NP seen when AUG1 was replaced with CUG most likely arose from non-AUG initiation at a CUG codon in a strong Kozak consensus (23,24), as the alternative mutation of AUG -> AGG blocked its formation (data not shown). Pairwise knockouts of the first three AUG codons in Eng/195 segment 5 also indicated leaky ribosomal scanning leading to context-dependent recognition of all three start sites (lanes 6 and 7). Creation of the equivalent mutations in the PR8 NP gene showed that similar rules applied; addition of uAUG led to production of a closely spaced NP doublet (Fig 2C, compare lanes 11 and 12), while mutating combinations of uAUG, AUG1 and AUG2 showed that the hierarchy of translation initiation potential *in vitro* was AUG1 > uAUG >> AUG2 (lanes 13-16). However, swapping the entire 5'-UTRs of Eng/195 and PR8 had little effect beyond that of the addition or omission of the uAUG (compare lanes 8 and 9, 17 and 18), suggesting that the nucleotide polymorphisms at positions 40, 43 and 44 were of little significance for initiation at AUG1.

The coupled *in vitro* transcription-translation system we used did not generate mRNAs with 5'-cap structures and nor was it optimised for KCl concentration, leading to the possibility of less accurate translation initiation than would occur in intact cells (25). We therefore tested NP expression after transfection of 293T cells with a corresponding set of plasmid constructs containing the first 201 nucleotides of segment 5 cDNA fused in frame to the green fluorescent protein (GFP) ORF (Fig 2D). This cloning strategy kept the 5'-end of the viral sequences intact but decreased the overall size of the expected polypeptides from ~

197 56 kDa to ~ 34 kDa, thus aiding separation of the various isoforms, as well as permitting their
198 detection by western blotting for GFP. In this system, all plasmids with an IAV UTR
199 produced a low abundance product with the same mobility as GFP (compare lanes 10 and
200 11). However, in addition to this, a construct with the WT PR8 UTR produced a single major
201 species while the WT Eng195 plasmid produced a clearly separated doublet (Fig 2D,
202 compare lanes 1 and 8, and lanes 11 and 18). As before, the relative abundance of the Eng195
203 upper doublet species was increased by a mutation that improved the Kozak consensus of the
204 uAUG while its synthesis was blocked by removal of the uAUG (lanes 2 and 3). Again,
205 similarly to the outcome of the *in vitro* translation experiments, mutation of AUG1 to CUG
206 produced a triplet species whose upper and lower constituents could be explained by
207 initiation at the uAUG and AUG2 in the absence of AUG1, as well as lower levels of CUG
208 codon-directed translation initiation at the mutated AUG1 codon (compare lane 4 with lanes
209 5-7). Analysis of the counterpart mutations in a PR8 background produced corresponding
210 results; introduction of the uAUG gave a doublet NP species (lane 12) while AUG2 was only
211 used for translation initiation after mutation of AUG1 to CUG had downregulated but not
212 abolished initiation at the canonical NP start site (lanes 13-16). Thus, the NP uAUG codon
213 was seen by scanning ribosomes in a cellular context as well as *in vitro* to produce eNP,
214 although AUG1 remained the preferred start site. In contrast to the cell-free setting,
215 translation initiation at AUG2 could only be detected in the absence of AUG1.
216
217 **eNP is functionally equivalent to canonical NP in supporting viral gene expression and**
218 **replication in cells**
219 Next, we examined the effect of a subset of these mutations on the ability of NP to
220 support viral gene expression, using an assay in which RNPs were reconstituted by
221 transfection of cells with plasmids encoding the three subunits of the viral RNA

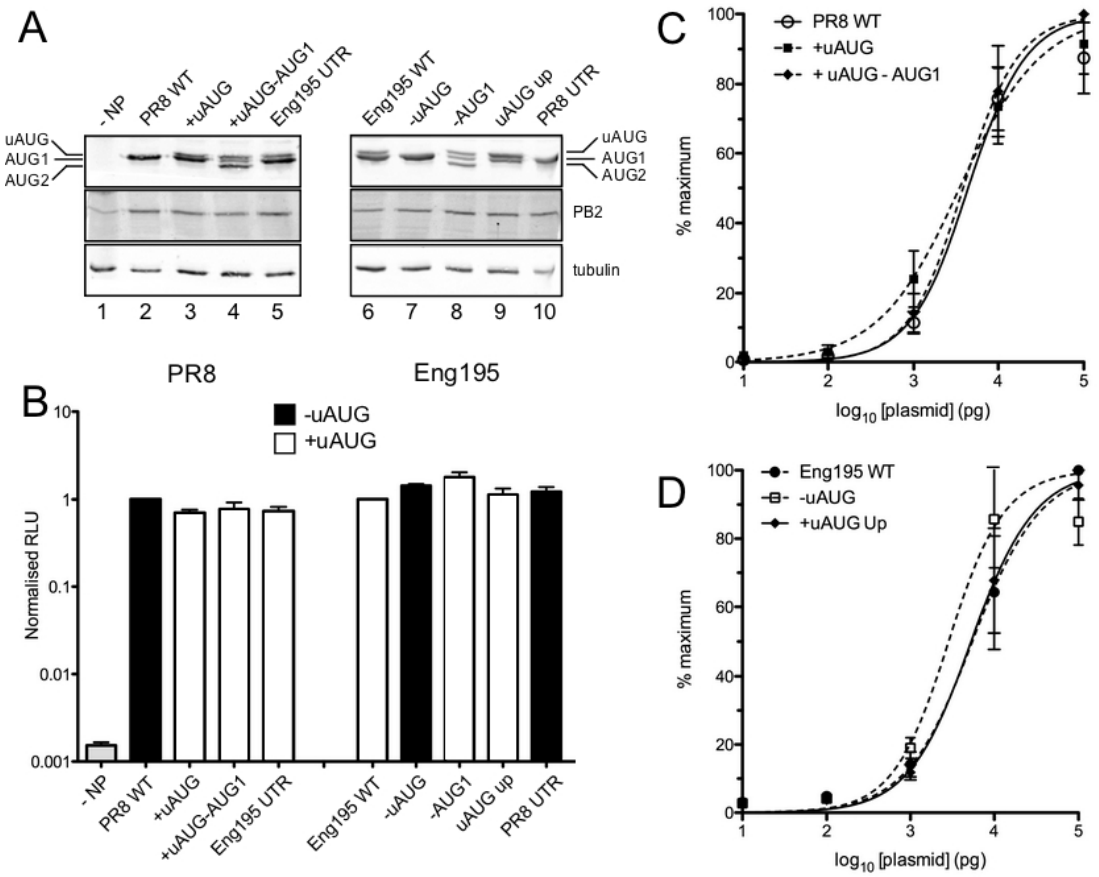

222

223 **Figure 3.** Ability of NP mutants to support viral gene expression in RNP reconstitution assays. 293T cells were
224 transfected with reverse genetics plasmids encoding the 3 polymerase proteins (from PR8 or Eng195 as
225 indicated), WT or mutant forms of NP and a vRNA-like reporter segment encoding luciferase, thus
226 reconstituting RNPs. (A) Cell lysates were analysed by SDS-PAGE and western blotting for the
227 indicated polypeptides. (B) Luciferase activity in the lysates was measured and normalised to the
228 amount seen with the corresponding WT gene. Data are the mean ± SEM of four independent
229 experiments. Differences between samples with a complete RNP were non-significant (repeated
230 measures ANOVA with Dunnett's multiple comparison test comparing against the matched WT) (C, D)
231 Luciferase activity was measured from RNP reconstitution assays in which the NP plasmid was titrated
232 and all other plasmids kept constant and normalised to the maximum activity within an individual
233 titration set. Data are the mean ± SEM of 3 (PR8 + uAUG – AUG1), 4 (all Eng195 data), 5 (PR8 +
234 uAUG) or 6 (WT PR8) independent experiments, curve fitted to a variable slope $\log_{10}$ [agonist]-
235 response model using Graphpad Prism. The 95% confidence limits of the estimated EC_{50} values within
236 groups overlapped, indicating non-significance (Table S4).

237

238 polymerase (3P) and WT or mutant copies of the NP gene (26,27), along with a vRNA-like
239 reporter segment with an antisense luciferase gene. First, NP expression was examined by
240 western blotting, where again, the presence of an uAUG codon in both PR8 and Eng195
241 backgrounds led to production of an NP doublet whose relative abundance varied according
242 to the strength of the uAUG Kozak consensus (Fig 3A). Reconstitution of both WT PR8 and
243 Eng195 RNPs led to around 300-fold increases in luciferase expression compared to a control
244 reaction lacking NP (Fig 3B). However, at a fixed dose of NP plasmid, all of the mutants had
245 comparable activity to their WT counterpart, with no more than 2-fold differences evident.
246 To provide a more sensitive examination of NP activity, we titrated the amounts of NP
247 plasmid and fitted the luciferase expression values to a variable slope dose-response enzyme
248 kinetic model. The resulting curves for both the PR8 and Eng195 sets of plasmids were very
249 similar (Fig 3C, D) and the estimated concentrations of plasmid required for half-maximal
250 activity were not significantly different. Thus, the precise identity of the N-terminus of NP
251 had little influence on viral gene expression, even at limiting amounts of the protein.
252 We then examined what effect the presence of the uAUG codon had on virus
253 replication *in vitro*. End-point titres following low multiplicity infection of MDCK cells with
254 WT PR8 or variants with the uAUG codon added to PR8 segment 5 were essentially the same
255 (Fig 4A, left hand bars). When the counterpart experiment was performed for viruses with
256 segment 5 from either Eng195 or another early isolate from the 2009 pandemic,
257 A/Halifax/210/2009 [SW210; (28)] (both as 7:1 reassortants on the PR8 background to
258 confer efficient infection of MDCK cells), removal of the uAUG codon with an A28C
259 mutation gave slight increases (4-5 fold) in average titres while replacing the normal Eng195
260 UTR with the PR8 sequence gave an 8-fold increase (Fig 4A, middle and right hand bars).
261 However, none of these differences were statistically significant. Western blot analysis of

lysates from cells infected at high multiplicity confirmed that the A28C polymorphism behaved as expected with respect to production or not of the two NP isoforms

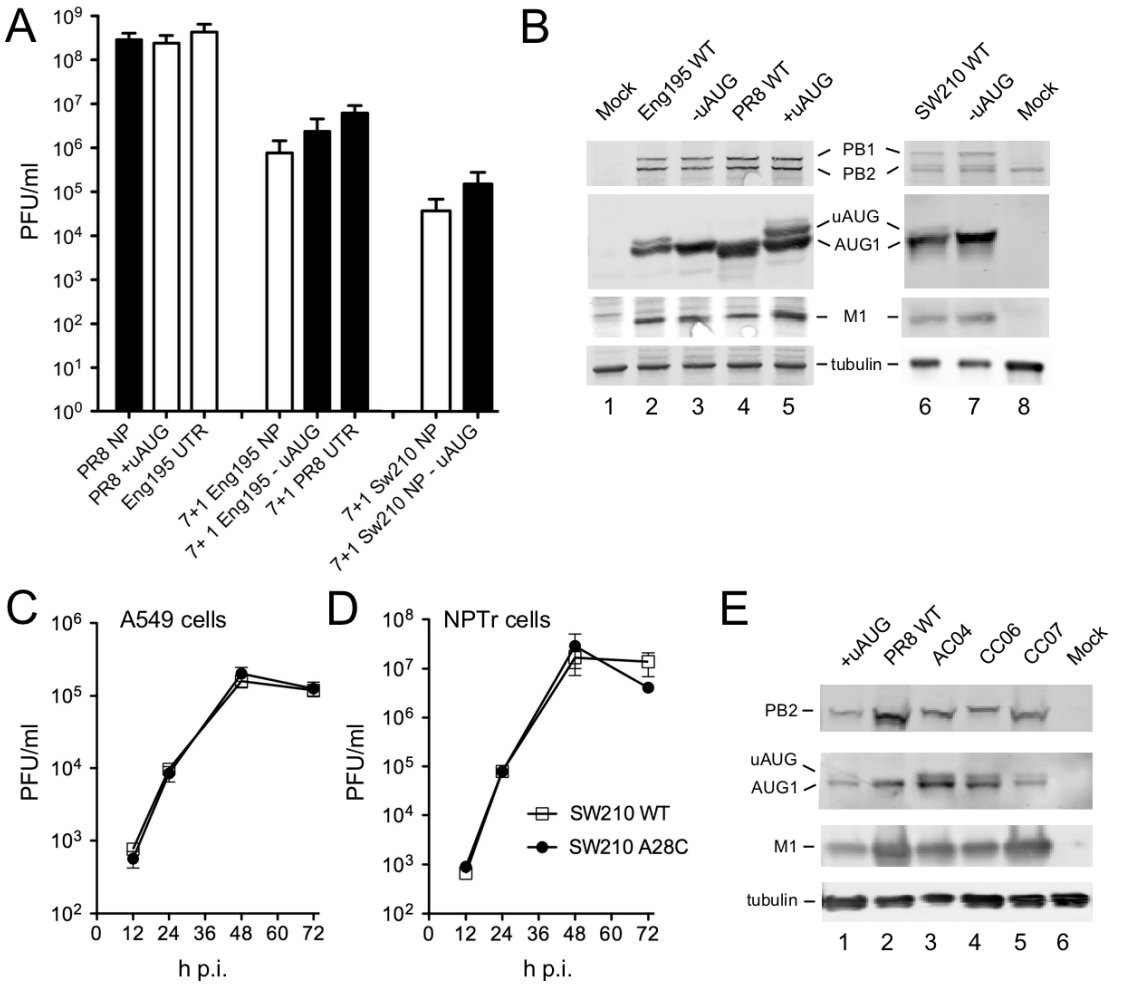

Figure 4. Expression and functional significance of eNP for virus replication *in vitro*. (A) MDCK cells were infected at an MOI of 0.01 with the indicated viruses and titres measured at 48 h p.i.. Data are the mean ± SEM of 4-5 independent experiments. Differences within groups were not statistically significant (PR8, Eng195; One way ANOVA with Tukey's post test, Sw210; *t*-test). (B) Cell lysates from A549 cells infected at an MOI of 5 and harvested at 24 h p.i. were analysed by SDS-PAGE and western blotting for the indicated polypeptides (uAUG/AUG1 = NP). (C, D) A549 or NPTr cells were infected an an MOI of 0.03 and samples titred at the indicated times p.i. Data are the mean ± SEM of three independent experiments. (E) Lysates from MDCK-SIAT cells infected with the indicated viruses at high MOI and harvested at 16 h p.i. were analysed by SDS-PAGE and western blotting for the indicated polypeptides.

in all virus backgrounds, without affecting synthesis of other viral structural proteins (Fig 4B). Since our clone of the Eng195 virus does not infect or replicate well in the continuous cell lines commonly used to study IAV replication, we tested the full SW210 virus under multicycle growth conditions in human A549 cells or swine new-born pig tracheal (NPTr) cells. WT and A28C mutant viruses replicated with almost identical kinetics in both cell types (Figs 4C, D). Thus the presence or absence of the segment 5 uAUG codon and expression of eNP had little effect on IAV replication *in vitro*.

Given the high proportion (97.9%) of pdm2009 isolates encoding uAUG (Table S1), we analysed three clinical isolates with known, limited *in vitro* passage histories (29) by western blotting following high multiplicity infection of MDCK-SIAT cells. All three viruses produced both NP and eNP (Fig 4E), further supporting the potential *in vivo* relevance of eNP expression.

The terminal regions of IAV genome segments are involved in vRNA packaging, via specific RNA signals (30). To test whether the mutations that added or subtracted the uAUG codon affected segment 5 packaging, RNA was extracted from independently grown stocks of WT or mutant viruses and the amount of segment 5 measured by qRT-PCR. The values obtained were then considered as a ratio to the plaque titre of the stocks, normalised to WT PR8, to produce a relative vRNA:PFU ratio. As a positive control for a virus with a packaging defect, we analysed a PR8 mutant with two clusters of synonymous mutations (9 nucleotide changes in total) introduced into the 5'-ends of segments 4 and 6, where bioinformatics analyses had predicted the likely location of packaging signals (31). The genome copy:PFU ratio of this "4c6c" virus was elevated by over 2 $\log_{10}$ compared to WT virus (Fig 5A). In contrast, introduction of the C28A mutation into PR8 had very little effect

299 on the quantity of segment 5 required to form an infectious unit. Replacement of PR8

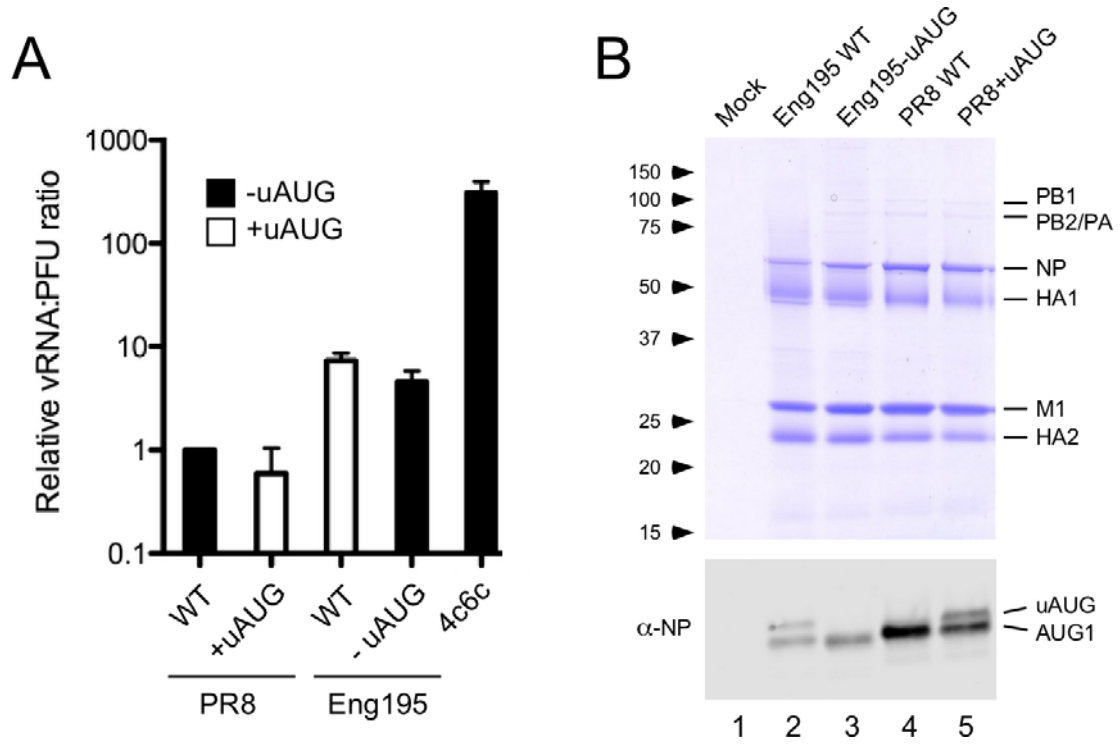

300

301 **Figure 5**. Virion composition of PR8 and PR8 7:1 reassortants containing the Eng195 segment 5 (Eng195). (A)
302 The segment 5 vRNA content of virus stocks of known infectious titre was determined by qRT-PCR and the
303 values used to derive genome:PFU ratios, normalised to that of WT PR8. Data are the mean ± range of two
304 independent replicates. (B) Aliquots of sucrose gradient purified virus or the corresponding fraction from
305 uninfected allantoic fluid was analysed by SDS-PAGE and (upper panel) Coomassie Blue staining or (lower
306 panel) western blotting for NP. The migration positions of molecular mass standards (kDa) and major viral
307 structural proteins are indicated. Note that the gel used for the lower panel was run further to separate the two
308 NP isoforms.

309

310 segment 5 with the corresponding WT Eng195 vRNA elevated the genome:PFU ratio by ~
311 10-fold, suggestive of a packaging incompatibility between the PR8 backbone and the
312 pdm2009 segment. However, addition of the A28C mutation into the Eng195 segment to
313 remove the uAUG codon did not worsen this phenotype. Overall therefore, the data did not
314 indicate any large effect of the A28C polymorphism on segment packaging.

315 To determine if eNP is incorporated into virus particles, virus stocks were grown in
316 embryonated hens' eggs and virions purified from allantoic fluid by pelleting through a

317 sucrose cushion followed by banding on a sucrose velocity gradient. SDS-PAGE and
318 Coomassie blue staining of the resulting material showed the presence of the expected major
319 viral structural proteins (Fig 5B, top panel). Re-analysis of the same material by western
320 blotting for NP under PAGE conditions sufficient to separate the two forms of NP clearly
321 showed the presence of both canonical and eNP in an approximately 2:1 ratio in viruses
322 where the uAUG codon was present (Fig 5B, bottom panel). Thus consistent with its
323 apparently normal function in minireplicon assays, eNP was incorporated into virus particles.
324

325 **The C28A polymorphism influences pathogenesis in mice**

326 To examine the role of eNP *in vivo*, the mouse model of IAV infection was used.
327 First, groups of BALB/c mice were infected with PR8 or the PR8:Eng195 segment 5
328 reassortant in either WT form or with the C28A polymorphism, and weight loss followed
329 over 5 days. Uninfected mice gained weight over time, while mice infected with WT PR8 lost
330 around 5% of their starting body weight (Fig 6A). Unexpectedly, the PR8 C28A mutant
331 induced significantly greater weight loss in the animals, resulting in an average loss of over
332 15%. Consistent with this, the PR8 C28A-infected mice showed increased clinical signs
333 compared to their WT-infected counterparts, including increased respiratory rate, lower
334 motility, more extreme staring of the coat and more emphatic hunching (data not shown).
335 Animals infected with the PR8:Eng195 segment 5 WT or A28C viruses did not show obvious
336 clinical signs or lose any substantial amount of weight over the 5 days (Fig 6A). At day 5, all
337 animals were sacrificed and the lungs collected for further analyses. When viral loads were
338 measured, both WT and C28A PR8 viruses gave titres of around 10^6 PFU/ml of homogenate
339 (Fig 6B). The reassortant virus with WT Eng195 segment 5 produced titres of around 10^5

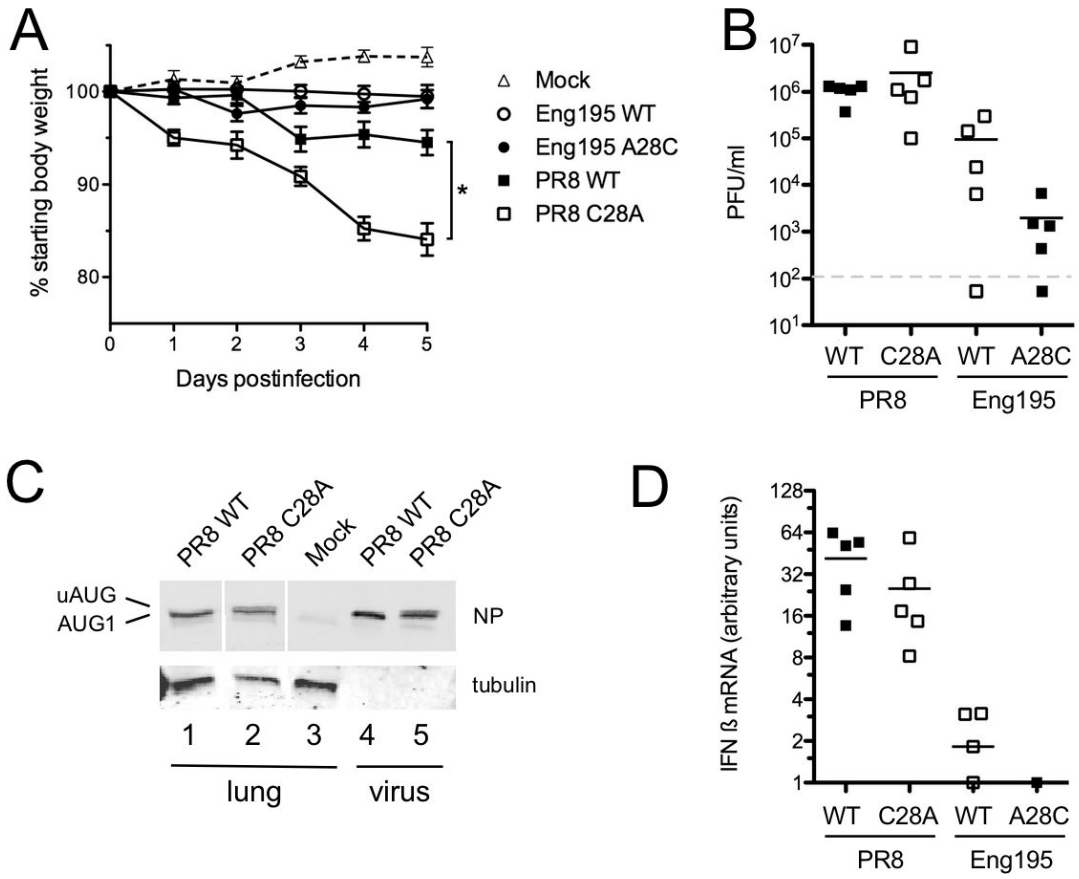

Figure 6. Pathogenesis of eNP-expressing viruses in Balb/c mice. Groups of 5 six-week old mice were infected with 200 PFU or PR8 viruses or 500 PFU of 7:1 PR8 reassortant viruses containing the Eng195 segment 5 (Eng195). (A) Body weight was measured daily for 5 days after infection. Data are plotted as the mean ± SEM. * $p < 0.05$ (One way ANOVA with Tukey's multiple comparison post test; WT PR8 versus PR8 C28A). (B) Animals were euthanised at day 5, the left lungs homogenised and virus titres determined. Dashed line indicates limit of detection. Differences between pairs of viruses were non-significant, as assessed by *t*-tests. (C) Aliquots of pooled lung homogenate (lung) or purified virus (virus) were analysed by SDS-PAGE and western blotting for the indicated proteins. (D) RNA was extracted from the left lung tip and IFN ß and GAPDH mRNA levels determined by qRT-PCR. IFN ß transcript was not detected in RNA from uninfected animals, so positive values were corrected for GAPDH levels and then expressed relative to the lowest samples that gave a C_t value (one animal each from WT and A28C Eng195 infections). Differences between virus pairs were not statistically significant (non-parametric *t*-tests).

PFU/ml, despite the lack of clinical signs of infection. However, the corresponding A28C mutant lacking the uAUG codon gave substantially lower (on average, almost 2 $\log_{10}$) titres, suggesting attenuated virus replication. Examination of lung homogenates by western

358 blotting for viral NP confirmed that the PR8 C28A virus expressed eNP *in vivo* (Fig 6C).
359 Neither form of NP could be detected in material from animals infected with the PR8:Eng195
360 reassortant viruses, most likely because of the lower levels of virus replication. To measure
361 innate immune response stimulation, levels of IFN-ß mRNA in the lung homogenates were
362 assessed by qRT-PCR. Transcripts were undetectable from mock infected mouse lung but
363 were clearly induced by PR8 virus infection (Fig 6D). However, despite the more severe
364 disease seen with the PR8 C28A virus, there was no significant difference between this and
365 WT virus samples. IFN-ß mRNA levels were substantially lower in animals infected with the
366 WT PR8:Eng195 virus and were undetectable in all but one animal infected with the A28C
367 mutant (Fig 6D); these differences plausibly correlated with virus load (Fig 6B). A similar
368 outcome was obtained when a broader array of cytokines and chemokines were analysed; few
369 differences of note between the PR8 pair of viruses and generally higher induction from WT
370 Eng195 than its A28C counterpart (Fig S6).
371 To assess histopathological changes in the mice, formalin-fixed lung sections were
372 stained with haematoxylin and eosin and examined by a veterinary pathologist. Changes
373 identified in infected mice were consistent with acute to subacute IAV infection; these were
374 characterised by degeneration and necrosis of epithelial cells lining airways, accompanied by
375 peribronchial and perivascular inflammation, as well as interstitial inflammation and necrosis
376 (Fig 7A and data not shown). The inflammatory infiltrate consisted of lymphocytes and
377 macrophages with fewer plasma cells, and rare neutrophils and eosinophils. When the slides
378 were scored blind for various pathological features, the C28A PR8 mutant gave generally
379 higher scores than WT PR8 in most categories (Fig 7B). Combining these scores along with a
380 consideration of the area of lung affected by pathological changes to give an overall score
381 showed significantly higher ($p < 0.05$, *t*-test) damage from the PR8 C28A virus (Table S5).

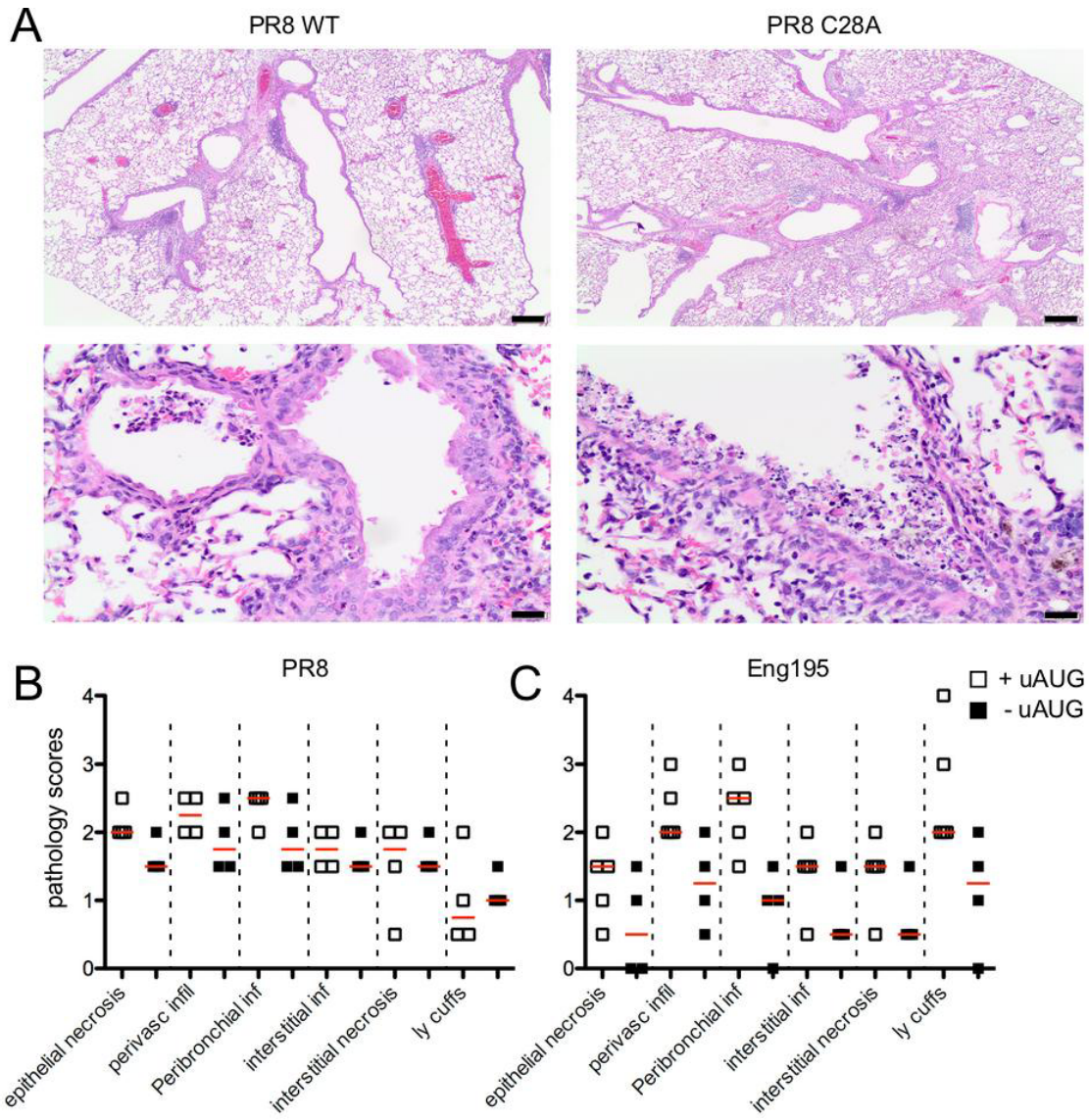

Figure 7. Histopathology of eNP-expressing viruses in Balb/c mice. At day 5 p.i., the right lung lobes of inoculated mice were collected, fixed, processed, and (A) stained with hematoxylin and eosin. Mock-infected mice showed no significant pathology (Table S4). Scale bars indicate 200 µm (top panels) or 20 µm (lower panels). (B, C) The severity of the pathology in individual lungs was assessed in a blind manner, and an overall score out of 4 for the various categories of damage was assigned (infil; infiltrate, inf; inflammation, ly; lymphocyte). Red bars indicate the median.

Conversely, the A28C Eng195 mutant gave lower average scores in all categories than its WT counterpart and an overall highly significant difference of $p < 0.005$ (Fig 7C and Table S4), confirming that mutation of the uAUG codon substantially attenuated virus pathogenicity.

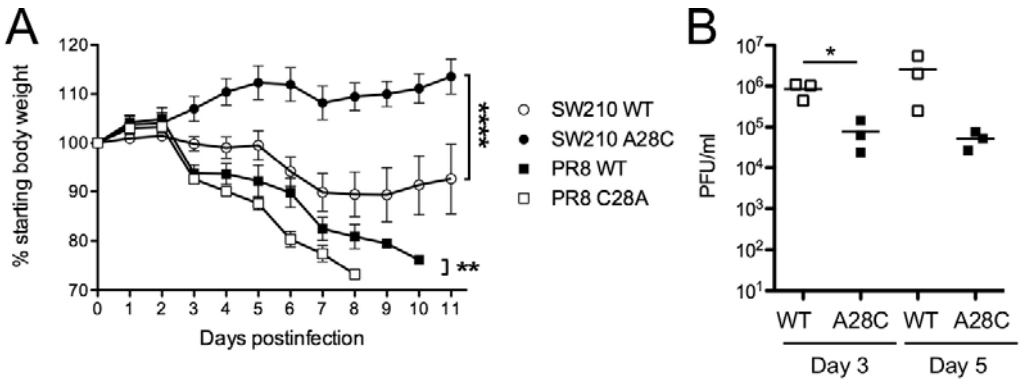

Figure 8. Pathogenesis of eNP-expressing viruses in CD-1 mice. Groups of 4-5 animals were infected with 10^4 PFU of PR8 viruses or $5x10^5$ PFU of SW210 viruses. (A) Body weight was measured daily for up to 11 days. Animals that met the humane end-point were euthanized earlier. Data are the mean ± SEM. ** $p < 0.01$, **** $p < 0.0001$ (*t*-tests between pairs of viruses). (B) For the SW210 pair of viruses, an additional six animals were included, and three animals were euthanized on each of days 3 and 5 p.i. for virus titres in lung homogenates to be determined. $p < 0.05$ (*t*-test between pairs of viruses on separate days).

BALB/c mice are biased towards Th2-type responses (32) and mouse strain-dependent variations in response to pdm2009 infection have been observed (33). Accordingly, to further test the effect of modulating NP start codons on viral pathogenicity, we examined the course of infection in the outbred CD-1 mouse strain after infection with a further two pairs of recombinant viruses differing only in the presence or absence of the segment 5 uAUG codon: a complete clone of the SW210 pdm2009 virus, and the St Jude Children's Hospital clone of PR8 (34). Infection with both WT and C28A mutant PR8 viruses led to severe weight loss from day 3 post infection onwards, resulting in all animals reaching a humane endpoint by day 11. However, consistent with the previous experiment, animals infected with the eNP-expressing mutant version of PR8 lost weight faster and died sooner (Fig 8A). Infection with WT SW210 virus led to animals losing around 10% of their body weight by day 7 followed by recovery from day 10. In contrast, the A28C derivative did not cause any evident disease (Fig 8A). Examination of lung titres taken at days 3 and 5 p.i. confirmed that the animals were infected but that the WT SW210 virus had replicated to titres

417 over 1 $\log_{10}$ higher than the A28C mutant (Fig 8B), indicating that removal of the NP uAUG
418 codon was attenuating *in vivo* in the background of an authentic pdm2009 virus. Thus, the
419 attenuating effect of altering the uAUG codon was consistent across virus strains and breeds
420 of mice.
421

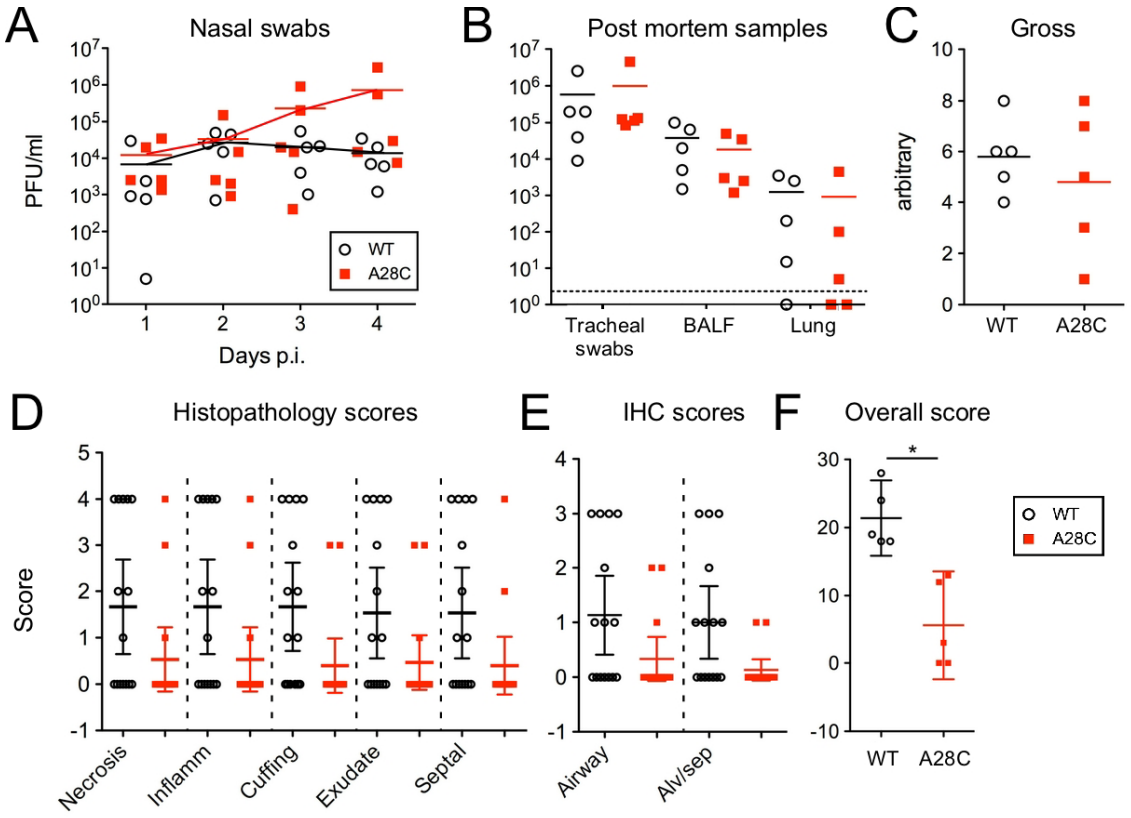

422

423 **Figure 9.** Pathogenesis of a pdm2009 virus with altered eNP expression in pigs. Inbred Babraham pigs were
424 challenged with WT or A28C Eng194 and (A, B) swabs and samples taken as indicated and titred for
425 virus. Dashed line indicates the limit of detection. (C) Following necropsy at day 4 p.i., lungs were
426 removed and scored for gross pathology. (D, E) Cut tissue sections were blinded and (D), stained with
427 H&E and scored for the indicated categories of pathology or (E), stained for NP and scored for the
428 quantity of viral antigen-positive cells. (F) – Iowa overall score, taking D and E together. * = $p < 0.05$
429 (Mann Whitney *t*-test).

430

431

432 **The C28A polymorphism influences pathogenesis in pigs**

With evidence from the mouse model of IAV infection that the presence of the segment 5 uAUG increased virulence, we tested whether this phenotype was replicated in pigs, where uAUG appeared to be strongly selected for in an evolutionary context. For this, we utilised a previously characterised challenge system using Babraham inbred pigs (35,36) for the Eng195 virus. Groups of animals were infected intranasally with 2.2×10^5 PFU of WT or A28C Eng195 and monitored for virus shedding by daily nasal swabs for 4 days. All animals shed detectable levels of virus for the duration of the experiment and although the average titres were higher from animals infected with the A28C virus at days 3 and 4 p.i. (Fig 9A), the data were variable and the differences were not statistically significant. At day 4 p.i., animals were euthanized and samples taken from the respiratory tract for virus titration. Titres were highest in tracheal swabs, intermediate in bronchiolar lavage fluid (BALF) and lowest in lung tissue homogenates, where not all samples were detectably positive (Fig 9B). As with the shedding data, there were no significant differences between the two viruses however. Examination of the animals' lungs showed areas of interstitial pneumonia and atelectasis mostly in the apical lung lobes (Fig S7). However, the overall macroscopic pathology scores between the two groups were also not significantly different (Fig 9C). To examine microscopic pathology, five tissue samples per right lung (two apical and one each from the medial, diaphragmatic and accessory lobes) were formalin fixed, processed into paraffin-wax and cut sections stained with H&E. Histopathological analysis showed multifocal interstitial pneumonia, attenuation/necrosis of bronchial and bronchiolar epithelial cells, presence of inflammatory cell infiltrates within the interalveolar septa and the alveolar lumen, and oedema (Fig 10A, B). These histopathological changes were scored across all sections by a board-certified veterinary pathologist according to five parameters: necrosis of the bronchiolar epithelium, airway inflammation, perivascular/bronchiolar cuffing, alveolar exudates, and septal inflammation (Table S6). Here, a clear difference between the two

458 viruses became apparent, with the A28C virus on average provoking lesser amounts of
459 damage to the lung by each criterion (Fig 9D). To assess virus spread within the lung,
460 sections were stained by IHC for IAV NP. Viral NP was observed mainly within the
461 bronchial and bronchiolar epithelial cells (Figure 10C), but also within inflammatory cells
462 inflitrating into the bronchiolar

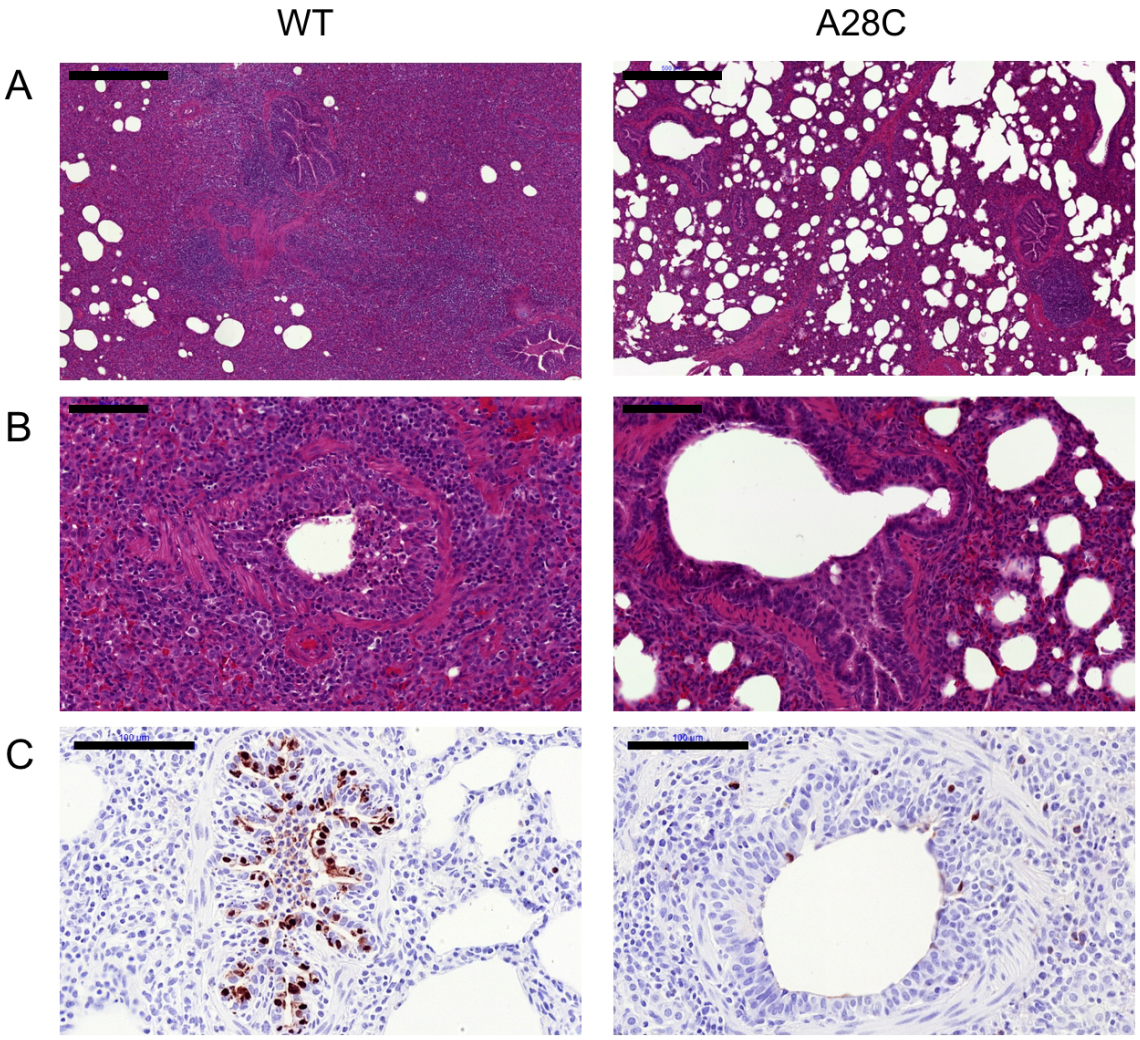

463

464 **Figure 10**. Histopathological analyses of pig lungs 4 days post challenge with WT and A28C Eng195 viruses.
465 Representative sections of lung stained with (A, B) H&E and imaged at low (scale bar = 500 µm) and high
466 (scale bar = 100 µm) magnification respectively or (C) stained for IAV NP (in brown) and counterstained with
467 haematoxylin. Scale bar = 100 µm.
468

lumen and alveolar spaces. NP-IHC staining was scored for the numbers of antigen-positive cells in airway epithelia and alveolar septa/lumens, showing reduced numbers of cells infected with the A28C mutant (Fig 9E). When histopathological and IHC scores were combined to provide an overall measure of pathology (the "Iowa" scale) (35), animals infected with the WT virus had consistent and significantly worse disease than those infected with the A28C mutant virus (Fig 9F). Thus, removing the uAUG codon from a pdm2009 virus led to reduced virulence in a biologically relevant large animal model of IAV infection.

Discussion

The pdm2009 virus possesses several genetic features which might have explained its unexpectedly mild disease characteristics in humans, including an avian IAV-like signature at PB2 residue 627 and truncated PB1-F2, PA-X and NS1 genes. However, artificially altering these sequences to what could reasonably be predicted to be a more pathogenic form and testing them in animal models of infection has generally failed to support a causative role in disease attenuation (6,37-43). Here, we investigated another genetic quirk of the pdm2009 virus; the presence of an extra in-frame start codon in the 5'-UTR of the NP gene. We found that this uAUG originally emerged in classical swine viruses circulating in the early 1960s, before being inherited by various reassortant lineages of viruses including the pdm2009 strain. We showed that the uAUG codon is used for translation initiation to produce two isoforms of NP in infected cells, in a roughly 3:1 ratio of "normal" and "extended" [eNP] polypeptides. This had little apparent functional consequence *in vitro*, either for viral gene expression (something that NP plays a crucial role in) or for overall virus replication. However, while the presence or absence of the uAUG did affect pathogenicity in mice and in pigs, it acted to increase rather than decrease virulence in both animal models of infection. Importantly, this included pigs, where the human pandemic strain originated. Thus, once

494 again, investigation of an unusual genetic feature of the pdm2009 virus has not supported the
495 simple hypothesis of an attenuating role in virulence.

496 A previous study has examined the functional significance of the segment 5 uAUG;
497 the authors did not directly determine whether it was actually used for translation initiation,
498 but using RNP reconstitution assays, they concluded that its presence significantly influenced
499 viral transcriptional activity, albeit only by around 2-fold (7). Here, we saw similar
500 magnitude effects, but without achieving statistical significance (Fig 2). We consider such
501 small fluctuations in minireplicon activity unlikely to have much biological consequence;
502 viruses with the same mutations replicated similarly in a variety of *in vitro* settings and had
503 no obvious deficits in gene expression (Fig 3). The question therefore remains, of how the
504 presence of the uAUG might enhance virulence. Whilst it is difficult to rule out subtle effects
505 arising directly from the UTR mutation (*e.g.* on segment 5 RNA synthesis or packaging),
506 these were normal as far as we could measure (Figs 4, 5). Instead, we prefer the hypothesis
507 that the *in vivo* phenotypic change results from the expression of a new isoform of NP. The
508 question then arises of how the function of the novel polypeptide varies from that of NP.

509 The N-terminal 20 amino acids of the canonical form of NP appear to be flexible, as
510 they are not visible in crystal structures of the whole protein (11,12,44). The primary function
511 attributed to this region of NP is that of a non-classical nuclear localization signal (ncNLS)
512 that binds cellular importin α (14,45-47). It is therefore possible that the addition of the 6
513 amino acids unique to the eNP sequence could affect interactions with importin α; the much
514 larger (50 amino acid) extension on the related influenza B virus NP has been shown to affect
515 nuclear localization of the protein (48). However, the structure of the IAV NP ncNLS bound
516 to importin α suggests that this would not necessarily be the case here, as it binds to the
517 relatively shallow minor NLS-binding site, leaving the N-terminus of the NP sequence free,
518 where a short extension could easily be accommodated (47). In addition, we did not see any

519 appreciable differences in NP intracellular trafficking arising from the presence or absence of
520 eNP during a time course of infection in A549 cells (data not shown). The N-terminal
521 disordered region of NP is also a target for regulatory post-translational modification, such as
522 phosphorylation (49-51) and sumoylation (52); again something that could potentially be
523 affected by the addition of the 6 amino acids unique to eNP. However, the post translational
524 modifications only occur on a small fraction of the NP molecules in the cell and would
525 presumably still occur normally on canonical NP, which remains the most abundant isoform
526 in cells infected with a virus containing the uAUG codon. Thus, any changes to post
527 translational modification of eNP seem unlikely to be the primary cause of the phenotypic
528 effects seen here.

529 Our working hypothesis is therefore that acquisition of the segment 5 uAUG codon
530 represents a gain-of-function mutation for porcine IAV, reflecting a novel function for eNP
531 versus NP. Since NP has not been convincingly associated with any intrinsic enzymatic
532 activity, this would most simply be explained by the additional sequence mediating a new (or
533 stronger) interaction with a cellular binding partner that affects the outcome of *in vivo*
534 infection, but without affecting virus replication *in vitro*, at least in the cell lines tested. At
535 present, we do not have candidates for such a cellular factor and further experimentation is
536 required to identify these. Another question that remains to be answered is whether eNP
537 modulates pathogenesis through incorporation into viral RNPs, or as an isolated protein.

538 We found through evolutionary analyses that the segment 5 uAUG is primarily a trait
539 associated with virus strains of swine origin, where its recurrent emergence and fixation in
540 the major swine virus lineage implies it provides a host-specific selective advantage. This
541 hypothesis is consistent with the reduced virulence exhibited by pdm2009 virus engineered to
542 lack the uAUG codon (Figs 9, 10). Whether the uAUG codon provides a selective advantage
543 in the human host is also unclear, but the sporadic emergence of the uAUG in humans prior

544 to 2009 without provoking a selective sweep implies these events, and its dissemination in
545 2009, were driven by founder effect. However, its subsequent maintenance in the human
546 pdm2009 lineage (Table S2) gives no sign that it is being selected against in humans.
547 In summary, we have characterised a swine host-specific mutation in the 5'UTR of
548 IAV segment 5 which introduces an alternative start codon in frame with the NP ORF that
549 adds 6 amino acids to the N-terminus of the protein. This mutation modulates virulence in
550 mice and pigs, and was introduced to the human population via the 2009 pandemic. This
551 knowledge adds to our ability to understand and predict IAV virulence in specific hosts and
552 furthermore, suggests that the tendency for IAV sequencing efforts to disregard the viral
553 UTRs may be missing useful information.
554

555 **Materials and Methods**

556 *Bioinformatics*

557 On 31 Jan 2019, all full-length NP nucleotide sequences of IAV (any host, any location, any
558 year) were downloaded from Genbank via the NCBI Influenza Virus Resource database (53).
559 The sequences were named using the schema:
560 ">{serotype}_{host}_{accession}_{strain}_{country}_{year}/{month}/{day}_{segname}".
561 50471 sequences in total were downloaded and of these there were 48288 with known
562 subtype, host, country and year. These were screened for duplicates and quality (number of
563 ambiguities), leaving 48245 good quality sequences which were padded with 10 codons (30
564 nucleotides) and then roughly aligned for further processing. However, although these
565 sequences were tagged as 'full length', not all of them reported sequence before the usual NP
566 start codon, leaving 33622 which had 5'UTR data suitable for analysis, representing 69.7%
567 of the good quality sequences. In order to determine in which major lineages the sequences
568 with upstream start codons occur, a stratified subsampling was performed, based on a

maximum of 1 sample per joint category of host + subtype + country or state (if USA, Canada, China or Russia) + year + upstream start codon. This type of subsampling retains the diversity of hosts, subtypes, locations, dates and start codons but will skew the percentages of hosts vs start codons. The subsampling resulted in a data set of 6242 sequences, which were aligned using MUSCLE in MEGA and manually adjusted (at the far 3' end of the coding region which was not guaranteed to be complete by the process).

To construct phylogenetic trees, phylogeny was calculated from the stratified subsample of 6242 sequences using RAxML with the GTR model allowing for a gamma distribution of variable site rates and 100 bootstraps. Detailed time-resolved phylogenetic trees of selected lineages or clades of the 6242 sequences dataset were inferred with BEAST (1.10.4) (54) using the SRD06 codon partitioned nucleotide model with uncorrelated relaxed log normal clock models and the constant population size or skygrid tree priors. Per lineage or clade, 1000 trees were sampled from the resulting posterior distribution of trees (after 10% burn-in). For each selected clade or lineage, the start codon was mapped as a binary variable (Conventional or Upstream) onto the set of 1000 posterior trees using a discrete trait asymmetric model in BEAST, resulting in a set of 10,000 trees (approximately 10 mappings per original tree), which were summarised to a maximum clade credibility tree using TreeAnnotator

Plasmids and antisera.

Each of the eight IAV segments used throughout were encoded on IAV reverse gene plasmids containing bi-directional RNA polymerase I and II promoters. Two different PR8 strains were used: most experiments used an MDCK-adapted variant of the UK National Institute of Biological Standards and Control vaccine strain of PR8 (55), while data shown in figure 7 used an egg-adapted PR8 strain described previously (28,34). Plasmids for the

A/England/195/2009 (Eng/195; an early UK pdm09 strain) are described in (22), while those for A/Halifax/210/2009 (SW210; an early pandemic isolate from the Queen Elizabeth II Hospital, Halifax, Nova Scotia, Canada) are described in (56). A plasmid encoding a gene fusion between the 5'-201 nucleotides of PR8 segment 5 and GFP was made by PCR-cloning the appropriate IAV sequence into pEGFP-1 (Clontech), followed by oligonucleotide-directed PCR mutagenesis (using standard protocols) to remove the A of the GFP AUG codon. Nucleotide substitutions in the segment 5 plasmids to modify AUG motifs were made by further rounds of oligonucleotide-directed mutagenesis. To create the 4c6c PR8 virus with a genome packaging defect, codons 546-548 of the PR8 HA gene were synonymously mutated to **t**T**a**GG**t**GC**c** and codons 451 to 453 of PR8 NA were mutated to **tca**AT**a**GA**t** (altered nucleotides indicated in lower case bold, all sequences given in (+) sense). Primer sequences are available on request. Sequence modifications to plasmids were confirmed by commercial Sanger sequencing (GATC, Eurofins Genomics) before being used in downstream experiments.

For western blotting, purchased antisera used were: mouse monoclonal anti-GFP (clone JL8, Clontech), rat monoclonal anti-ß tubulin (clone YL1/2, Abd-Serotech) and mouse monoclonal anti-IAV NP (clone AA5H, Abd-Serotech). In-house rabbit polyclonal antisera raised against IAV PB1, PB2, NP and M1 have been previously described (57-59). Secondary antibodies labelled with infrared-fluorescent dyes were obtained from Fisher. For IHC staining of cut tissue sections, mouse monoclonal anti-NP (hybridoma HB-65 from ATCC (Manassas, VA, USA)) was used.

Viruses.

Virus rescues were performed as previously described (27,60). Briefly, 293T cells were transfected with 250ng each of the 8 plasmids from a viral reverse genetics set (or no

segment 5 as a negative control), with 1µg/ml tosyl phenylalanyl chloromethyl ketone (TPCK)-treated trypsin added at 48 hours post-transfection. At 72-96 hours post-transfection, supernatants were harvested and either passaged on MDCK cells in serum free medium with 1µg/ml TPCK-treated trypsin, or 100 µl was inoculated into the allantoic cavity of 12 day-old embryonated hen's eggs, the allantoic fluid of which was harvested at day 14 and aliquoted as virus stock. Titres were determined by plaque assay on MDCK (PR8; at 37°C) or MDCK-SIAT cells (61)(Eng/195; at 35°C). Plaques on MDCK cells were typically visualized by toluidine blue staining, while plaques on MDCK-SIAT cells were immunostained for viral NP. The presence of the desired mutations in the virus genome was confirmed by RT-PCR and Sanger sequencing of RNA isolated from the virus stocks. Early-passage H1N1 pdm2009 clinical isolates A/Nottingham/Adult-Community04/2009 (AC04), A/Nottingham/Child-Community06/2009 (CC06) and A/Nottingham/Child-Community07/2009 (CC07) were isolated and passaged twice on MDCK cells as described (29).

Cells and transfection methods

293T, MDCK, A549, and NPTr cells were grown in DMEM supplemented with 10% FBS and 1% penicillin and streptomycin (Fisher) and maintained by twice weekly passage. IAV minireplicon assays were performed as described (27). Briefly, unless otherwise stated, 50ng each of pDUAL plasmids encoding segment 1,2, 3 and 5 and 20ng of a construct that expresses an IAV-like vRNA encoding luciferase were transfected into 293T cells in 24 well format. Transfected cells were harvested in 100 µl cell culture lysis reagent (Promega) and 60 µl supernatants were mixed with 25 µl 6mM beetle luciferin (Promega). Luminescence was measured on a GloMax luminometer (Promega). Assays were performed using four technical replicates for each datapoint as well as at least three biological repeats.

644 *Protein methods*

645 *In vitro* translation reactions were performed using coupled bacteriophage T7 RNA
646 polymerase transcription-rabbit reticulocyte lysate translation reactions as per the
647 manufacturer's instructions (Promega TNT). Samples were radiolabelled with ^{35}S-methionine
648 (Perkin Elmer) and detected by SDS-PAGE and autoradiography. To separate eNP and NP,
649 samples were loaded onto 10% pre-cast gels (BioRad) and run until the 50kDa ladder marker
650 had just run off the bottom of the gel. For western blotting, wet transfers were performed,
651 membranes were blocked with 5% milk for 30-60 minutes then incubated with specific
652 antibodies in 2% BSA at 4ºC overnight. The next day, membranes were incubated with
653 secondary anti-rabbit or anti-mouse IgG antibodies conjugated to fluorophore AlexaFluor
654 680 or 800 as required, before imaging using a LiCor Odyssey FC.

655 To purify virus, allantoic fluid was clarified twice by centrifugation for 10 min at
656 2100 x g, then loaded onto a 30% sucrose/PBS cushion and spun at 30,000 rpm using an
657 SW28Ti Beckman rotor for 1 hour and 30 min at 4°C. The resulting pellet was gently washed
658 once with 500 µl of PBS to remove residual sucrose and re-suspended back in 50 µl of PBS
659 overnight. The virus was further purified by ultracentrifugation through a 15-60% sucrose
660 gradient (in PBS) spun at 38,000rpm for 40 min using a Beckman SA41Ti rotor at 4°C. The
661 virus band was extracted from the gradient using a syringe and virus pelleted by
662 centrifugation at 30,000 rpm for 90 min at 4°C before being resuspended as above.

663 For cytokine arrays of mouse lung homogenates, 20 µl of lung homogenate per mouse
664 was collected and pooled within groups. Cytokines were then measured using Proteome
665 Profiler Mouse Cytokine Array Kit (R&D Biosystems) according to manufacturer's
666 instructions. Arrays were imaged and spot intensities quantified using a LI-COR Odyssey
667 Infrared Imaging System (LI-COR, Cambridge, UK). Following normalization to within-

assay control spots values were plotted as fold increase in cytokine expression over mock-infected animals.

Ethics statement.

Animal experimentation was approved by the Roslin Institute Animal Welfare and Ethical Review Board, the Pirbright Institute Ethical Review Board under the authority of Home Office project licences (60/4479 and 70/7505 respectively) within the terms and conditions of the UK Home Office "Animals (Scientific Procedures) Act 1986" and associated guidelines, or in compliance with the guidelines of the Canadian Council on Animal Care (CCAC) as outlined in the Care and Use of Experimental Animals, Vol. 1, 2nd Edn. (1993). In this case, the animal care protocol was approved by the University of Ottawa Animal Care Committee (Protocol Number: BMI-85) and all efforts were made to minimize suffering and mice were euthanized at humane end-points, if infection resulted in greater than 30% body weight loss plus respiratory distress.

Mouse infections.

BALB/c mice were purchased from Harlan UK Ltd (Oxon, UK), CD-1 mice were purchased from Charles River Laboratories, (Montreal, Quebec, Canada). Five- to 12-week-old female mice were used in all experiments. A group size of 5 was used as based on variance observed in previous experiments, this was expected to give 80% power to detect a statistically significant difference of 6% weight loss at the 5% significance level. Mice were anaesthetized using isoflurane (Merial Animal Health Ltd) and infected intranasally with virus in 40 µl serum-free DMEM. Mice were weighed daily and assessed for visual signs of clinical disease, including inactivity, ruffled fur and laboured breathing. At day 5-post infection, mice were euthanized by CO_2 asphyxiation. Virus titration and RNA extraction

693 and qRT-PCR was undertaken as previously described (62). Briefly, left lung homogenates
694 were collected in 500 µl DMEM and homogenised using a Qiagen TissueLyser II. For virus
695 titration, standard plaque assays on MDCK cells were performed and the remaining
696 supernatant was used for RNA quantification. RNA was extracted using a Qiagen Viral RNA
697 mini kit according to manufacturer's instructions and DNAse treated using Promega RQ1-
698 RNAse free DNAse. RT-qPCR was undertaken using a BioLine Sensifast one step RT-qPCR
699 kit with modified cycling conditions of 45°C for 10 minutes, 95°C for 2 minutes, then 40
700 cycles of 95°C for 10s and 60°C for 30s. Primer sequences are given in Table 2. For
701 histopathological analysis,
702
703 **Table 2.** Sequences of primers used for RT-qPCR**.**
704

Gene	Polarity	Sequence
Seg2	Sense	GGAACAGGATACACCATGGA
	Antisense	AGTGGYCCATCAATCGGGTT
Seg 5	Sense	ATCATGGCGTCTCAAGGCAC
	Antisense	CCGACGGATGCTCTGATTTC
GAPDH	Sense	CTACCCCCAATGTGTCCGTCG
	Antisense	GATGCCTGCTTCACCACCTTC
IFN-β	Sense	CACAGCCCTCTCCATCAACT
	Antisense	GCATCTTCTCCGTCATCTCC

705
706 the four lobes of the right lung were inflated with and then immersed in 10% neutral buffered
707 formalin (Sigma-Aldrich) until fixed, then processed using routine methods and embedded in
708 paraffin blocks. 5 µm thin section were then cut and stained with haematoxylin and eosin for
709 histological examination. Sections were assessed (blinded) by a veterinary pathologist
710 (PMB). The individual pathology features assessed were damage to the airway epithelium
711 (degeneration, necrosis and repair), perivascular inflammation, peribronchi/bronchiolar
712 inflammation, interstitial inflammation, interstitial necrosis and type II pneumocyte

713 hyperplasia. Each feature was scored from 1 (mild) to 3 (marked). The percentage of lung
714 affected was also noted.
715
716 *Pig infection model*
717 Ten 12-14 wk old Babraham large white inbred pigs (average weight 30 kg) were obtained
718 from the Pirbright Institute/ Animal Plant Health Agency. Pigs were screened for absence of
719 influenza infection by hemagglutination inhibition using four swine IAV antigens. Pigs were
720 randomly divided into two groups and were inoculated intranasally with 2.2×10^5 PFU virus.
721 Previous experiments showed that the standard deviation in viral shedding within groups is
722 around 0.8 $\log_{10}$ pfu/ml, so a group size of five pigs was sufficient to detect a difference in
723 viral shedding with 80% power and 95% confidence (power and sample size calculation for a
724 one-way ANOVA with three groups in Minitab 17). Two milliliters were administered to
725 each nostril using a MAD300 mucosal atomization device (Wolfe Tory Medical). Four nasal
726 swabs (two per nostril) were taken daily after the challenge. Two nasal swabs were placed in
727 2 ml virus transport medium for the quantification of viral load by plaque assay as previously
728 described (63). The other two nasal swab samples were put directly into TRIzol (Invitrogen,
729 ThermoFisher Scientific, UK) for subsequent RNA isolation according to the manufacturer's
730 instructions. Animals were humanely killed 5 d post challenge. At post mortem, the lungs
731 were removed, and photographs taken of the dorsal and ventral aspects. Macroscopic
732 pathology was scored blind, as previously reported (64). Tracheal swabs, bronchoalveolar
733 lavage and the accessory lobe were collected to determine the viral load in the lower
734 respiratory tract by plaque assay. In brief, the accessory lobe was cut into small pieces and
735 homogenised with a gentleMACS Octo Dissociator (Miltenyi Biotec) using C tubes (Miltenyi
736 Biotec) in ice cold Dulbecco's PBS supplemented with 0.1% BSA. The lung homogenates
737 (10% w/v) were centrifuged and the clarified supernatant was used to determine the viral load

and for RNA isolation. The tracheal swabs were processed like the nasal swabs. BALF was collected as previously described (63) and cell-free supernatant used to determine viral load. For histopathology, five lung tissue samples per animal from the right lung (two pieces from the apical, one from the medial, one from the diaphragmatic and one from the accessory lobe) were collected into 10% neutral buffered formalin for routine histological processing at the University of Surrey. Formalin-fixed tissues were paraffin wax–embedded, and 4 µm sections were cut and stained with H&E. Immunohistochemical staining of IAV NP was performed in 4 µm tissue sections as previously described (65). Histopathological changes in the stained lung tissue sections were scored by a veterinary pathologist blinded to the treatment group. Lung histopathology was scored using five parameters (necrosis of the bronchiolar epithelium, airway inflammation, perivascular/bronchiolar cuffing, alveolar exudates and septal inflammation) scored on a five-point scale of 0 to 4 and then summed to give a total slide score ranging from 0 to 20 and a total animal score from 0 to 100 (66). The Iowa system includes both histological lesions and immunohistochemical staining for NP (35). Sequencing of segment 5 from virus-positive samples from pigs confirmed that viruses produced during infection encoded uAUG or not, as expected (data not shown).

Numerical analyses

The numbers of replicates for each experiment are defined in the figure legends. Independent experiments are defined as replicates carried out on different days. Scatter plot data points indicate data points from individual samples. Statistical analyses were chosen according to published advice (67) and unless otherwise stated, were performed using Graphpad Prism.

Acknowledgements

We thank Dr Ben Killingley for clinical virus isolates, Dr Ed Hutchinson for critical comments, the Easter Bush Pathology Service staff for assistance and the animal staff at the Roslin and Pirbright Institutes and University of Ottawa for animal care.

Disclosures

JSN-V-T is currently seconded to the Department of Health and Social Care (DHSC), England. The views expressed in this manuscript are those of the authors and not necessarily those of DHSC.

Funding information

This work was funded by Institute Strategic Programme Grants (BB/J01446X/1 and BB/P013740/1) from the UK Biotechnology and Biological Sciences Research Council (BBSRC) to PD, BMD, PMB, EG and SJL, as well as BBS/E/I/00007030 and BBS/E/I/00007031 to ET and PMB, a National Institute for Health Research (Grant: 09/85 FLU-DRP) to JSN-V-T, a Canadian Institutes of Health Research (CIHR) Pandemic Preparedness Team grant (no. TPA-90188) to the CIHR Canadian Influenza Pathogenesis Team (EGB) and a CIHR Institute of Infection and Immunity (http://www.cihr-irsc.gc.ca/) operating grant (MOP-74526) to EGB. EG is supported by a Wellcome Trust/ Royal Society Sir Henry Dale Fellowship (211222/Z/18/Z), while SJL is supported by a University of Edinburgh Chancellor's Fellowship. KK was supported by a Wellcome Trust PhD studentship (no. 086157).

Bibliography

1. Dawood FS, Iuliano AD, Reed C, Meltzer MI, Shay DK, Cheng PY, et al. Estimated global mortality associated with the first 12 months of 2009 pandemic influenza A H1N1 virus circulation: A modelling study. Lancet Infect Dis. 2012 Sep 1;12(9):687–95.

2. Simonsen L, Spreeuwenberg P, Lustig R, Taylor RJ, Fleming DM, Kroneman M, et al. Global Mortality Estimates for the 2009 Influenza Pandemic from the GLaMOR Project: A Modeling Study. Hay SI, editor. PLoS Med. Public Library of Science; 2013 Nov 1;10(11):e1001558.

3. Garten RJ, Garten RJ, Davis CT, Davis CT, Russell CA, Russell CA, et al. Antigenic and genetic characteristics of swine-origin 2009 A(H1N1) influenza viruses circulating in humans. Science. 2009 Jul 10;325(5937):197–201.

4. Jagger BW, Jagger BW, Wise HM, Wise HM, Kash JC, Kash JC, et al. An overlapping protein-coding region in influenza A virus segment 3 modulates the host response. Science. 2012 Jul 13;337(6091):199–204.

5. Shi M, Shi M, Jagger BW, Jagger BW, Wise HM, Wise HM, et al. Evolutionary conservation of the PA-X open reading frame in segment 3 of influenza A virus. J Virol. 2012 Nov;86(22):12411–3.

6. Hale BG, Steel J, Medina RA, Manicassamy B, Ye J, Hickman D, et al. Inefficient control of host gene expression by the 2009 pandemic H1N1 influenza A virus NS1 protein. J Virol. American Society for Microbiology; 2010 Jul;84(14):6909–22.

7. Wanitchang A, Wanitchang A, Patarasirin P, Patarasirin P, Jengarn J, Jengarn J, et al. Atypical characteristics of nucleoprotein of pandemic influenza virus H1N1 and their roles in reassortment restriction. Arch Virol. 2011 Jun;156(6):1031–40.

8. Portela A, Portela A, Digard P. The influenza virus nucleoprotein: a multifunctional RNA-binding protein pivotal to virus replication. J Gen Virol. 2002 Apr;83(Pt 4):723–34.

9. Eisfeld AJ, Neumann G, Kawaoka Y. At the centre: influenza A virus ribonucleoproteins. Nat Rev Microbiol. 2015 Jan;13(1):28–41.

10. Kukol A, Hughes DJ. Large-scale analysis of influenza A virus nucleoprotein sequence conservation reveals potential drug-target sites. Virology. 2014 Apr 1;454-455:40–7.

11. Ye Q, Krug RM, Tao YJ. The mechanism by which influenza A virus nucleoprotein forms oligomers and binds RNA. Nature. 2006 Dec 21;444(7122):1078–82.

12. Ng AK-L, Ketha KMV, Atreya CD, Zhang H, Tan K, Li Z, et al. Structure of the influenza virus A H5N1 nucleoprotein: implications for RNA binding, oligomerization, and vaccine design. BMC Cell Biol. 2008;9(10):22–3647.

13. O'Neill RE, Palese P. NPI-1, the human homolog of SRP-1, interacts with influenza virus nucleoprotein. 1995 Jan 10;206(1):116–25.

14. Neumann G, Neumann G, Castrucci MR, Castrucci MR, Kawaoka Y, Kawaoka Y. Nuclear import and export of influenza virus nucleoprotein. J Virol. 1997 Dec;71(12):9690–700.

15. Wu WW, Sun Y-HB, Panté N. Nuclear import of influenza A viral ribonucleoprotein complexes is mediated by two nuclear localization sequences on viral nucleoprotein. Virol J. BioMed Central Ltd; 2007 Jun 4;4(1):49.

16. Taubenberger JK, Kash JC. Influenza virus evolution, host adaptation, and pandemic formation. Cell Host Microbe. 2010 Jun 25;7(6):440–51.

17. Wang R, Taubenberger JK. Characterization of the noncoding regions of the 1918 influenza A H1N1 virus. J Virol. American Society for Microbiology Journals; 2014 Feb;88(3):1815–8.

18. Pulit-Penaloza JA, Belser JA, Tumpey TM, Maines TR. Sowing the Seeds of a Pandemic? Mammalian Pathogenicity and Transmissibility of H1 Variant Influenza Viruses from the Swine Reservoir. Trop Med Infect Dis. Multidisciplinary Digital Publishing Institute; 2019 Feb 27;4(1):41.

19. Zhu Q, Yang H, Chen W, Cao W, Zhong G, Jiao P, et al. A naturally occurring deletion in its NS gene contributes to the attenuation of an H5N1 swine influenza virus in chickens. J Virol. 2008 Jan;82(1):220–8.

20. Kozak M. Point mutations define a sequence flanking the AUG initiator codon that modulates translation by eukaryotic ribosomes. Cell. 1986 Jan 31;44(2):283–92.

21. Wise HM, Barbezange C, Jagger BW, Dalton RM, Gog JR, Curran MD, et al. Overlapping signals for translational regulation and packaging of influenza A virus segment 2. Nucleic Acids Research. 2011 Sep 1;39(17):7775–90.

22. Brookes DW, Miah S, Lackenby A, Hartgroves L, Barclay WS. Pandemic H1N1 2009 influenza virus with the H275Y oseltamivir resistance neuraminidase mutation shows a small compromise in enzyme activity and viral fitness. J Antimicrob Chemother. 2011 Mar;66(3):466–70.

23. Diaz de Arce AJ, Noderer WL, Wang CL. Complete motif analysis of sequence requirements for translation initiation at non-AUG start codons. Nucleic Acids Research. 2018 Jan 25;46(2):985–94.

24. Peabody DS. Translation initiation at non-AUG triplets in mammalian cells. J Biol Chem. 1989 Mar 25;264(9):5031–5.

25. Dasso MC, Jackson RJ. On the fidelity of mRNA translation in the nuclease-treated rabbit reticulocyte lysate system. Nucleic Acids Res. Oxford University Press; 1989 Apr 25;17(8):3129–44.

26. Huang TS, Palese P, Krystal M. Determination of influenza virus proteins required for genome replication. Journal of Virology. American Society for Microbiology (ASM); 1990 Nov;64(11):5669–73.

27. Wise HM, Foeglein Á, Sun J, Dalton RM, Patel S, Howard W, et al. A complicated message: Identification of a novel PB1-related protein translated from influenza A virus segment 2 mRNA. J Virol. 2009 Aug;83(16):8021–31.

28. Lin L, Li Y, Pyo H-M, Lu X, Raman SNT, Liu Q, et al. Identification of RNA helicase A as a cellular factor that interacts with influenza A virus NS1 protein and its role in the virus life cycle. J Virol. 5 ed. American Society for Microbiology Journals; 2012 Feb;86(4):1942–54.

29. Killingley B, Greatorex J, Digard P, Wise H, Garcia F, Varsani H, et al. The environmental deposition of influenza virus from patients infected with influenza A(H1N1)pdm09: Implications for infection prevention and control. Journal of Infection and Public Health. King Saud Bin Abdulaziz University for Health Sciences; 2015 Dec 1;:1–11.

30. Kirchbach von JC, Gog JR, Digard P. Genome packaging in influenza A virus. J Gen Virol. 2010 Feb;91(Pt 2):313–28.

31. Gog JR, Afonso EDS, Dalton RM, Leclercq I, Tiley L, Elton D, et al. Codon conservation in the influenza A virus genome defines RNA packaging signals. Nucleic Acids Research. Oxford University Press; 2007;35(6):1897–907.

32. Mills CD, Kincaid K, Alt JM, Heilman MJ, Hill AM. M-1/M-2 macrophages and the Th1/Th2 paradigm. J Immunol. 2000 Jun 15;164(12):6166–73.

33. Otte A, Gabriel G. 2009 pandemic H1N1 influenza A virus strains display differential pathogenicity in C57BL/6J but not BALB/c mice. Virulence. 2011 Nov;2(6):563–6.

34. Hoffmann E, Krauss S, Perez D, Webby R, Webster RG. Eight-plasmid system for rapid generation of influenza virus vaccines. Vaccine. 2002 Aug 19;20(25-26):3165–70.

35. Gauger PC, Vincent AL, Loving CL, Henningson JN, Lager KM, Janke BH, et al. Kinetics of lung lesion development and pro-inflammatory cytokine response in pigs with vaccine-associated enhanced respiratory disease induced by challenge with pandemic (2009) A/H1N1 influenza virus. Vet Pathol. 2012 Nov;49(6):900–12.

36. Tungatt K, Dolton G, Morgan SB, Attaf M, Fuller A, Whalley T, et al. Induction of influenza-specific local CD8 T-cells in the respiratory tract after aerosol delivery of vaccine antigen or virus in the Babraham inbred pig. Legge K, editor. PLoS Pathog. Public Library of Science; 2018 May;14(5):e1007017.

37. Zhu H, Wang J, Wang P, Song W, Zheng Z, Chen R, et al. Substitution of lysine at 627 position in PB2 protein does not change virulence of the 2009 pandemic H1N1 virus in mice. Virology. 2010 May 25;401(1):1–5.

38. Pena L, Vincent AL, Loving CL, Henningson JN, Lager KM, Lorusso A, et al. Restored PB1-F2 in the 2009 pandemic H1N1 influenza virus has minimal effects in swine. J Virol. American Society for Microbiology; 2012 May;86(10):5523–32.

900 39. Hai R, Schmolke M, Varga ZT, Manicassamy B, Wang TT, Belser JA, et al. PB1-F2
901 expression by the 2009 pandemic H1N1 influenza virus has minimal impact on
902 virulence in animal models. J Virol. 2010 May;84(9):4442–50.

903 40. Gao H, Sun Y, Hu J, Qi L, Wang J, Xiong X, et al. The contribution of PA-X to the
904 virulence of pandemic 2009 H1N1 and highly pathogenic H5N1 avian influenza
905 viruses. Sci Rep. Nature Publishing Group; 2015 Feb 5;5(1):8262.

906 41. Lee J, Yu H, Li Y, Ma J, Lang Y, Duff M, et al. Impacts of different expressions of
907 PA-X protein on 2009 pandemic H1N1 virus replication, pathogenicity and host
908 immune responses. Virology. 2017 Apr;504:25–35.

909 42. Jagger BW, Memoli MJ, Sheng Z-M, Qi L, Hrabal RJ, Allen GL, et al. The PB2-
910 E627K mutation attenuates viruses containing the 2009 H1N1 influenza pandemic
911 polymerase. 2010 Apr;1(1).

912 43. Tu J, Guo J, Zhang A, Zhang W, Zhao Z, Zhou H, et al. Effects of the C-terminal
913 truncation in NS1 protein of the 2009 pandemic H1N1 influenza virus on host gene
914 expression. Pekosz A, editor. PLoS ONE. Public Library of Science;
915 2011;6(10):e26175.

916 44. Chenavas S, Estrozi LF, Slama-Schwok A, Delmas B, Di Primo C, Baudin F, et al.
917 Monomeric nucleoprotein of influenza A virus. 2013 Mar 1;9(3):e1003275.

918 45. Wang P, Palese P, O'Neill RE. The NPI-1/NPI-3 (karyopherin alpha) binding site on
919 the influenza a virus nucleoprotein NP is a nonconventional nuclear localization
920 signal. J Virol. 1997 Mar;71(3):1850–6.

921 46. Cros JF, García-Sastre A, Palese P. An unconventional NLS is critical for the nuclear
922 import of the influenza A virus nucleoprotein and ribonucleoprotein. Traffic.
923 Blackwell Publishing Ltd; 2005 Mar;6(3):205–13.

924 47. Nakada R, Hirano H, Matsuura Y. Structure of importin-α bound to a non-classical
925 nuclear localization signal of the influenza A virus nucleoprotein. Sci Rep. Nature
926 Publishing Group; 2015 Oct 12;5:15055.

927 48. Sherry L, Smith M, Davidson S, Jackson D. The N terminus of the influenza B virus
928 nucleoprotein is essential for virus viability, nuclear localization, and optimal
929 transcription and replication of the viral genome. García-Sastre A, editor. J Virol. 5 ed.
930 American Society for Microbiology Journals; 2014 Nov;88(21):12326–38.

931 49. Arrese M, Portela A. Serine 3 is critical for phosphorylation at the N-terminal end of
932 the nucleoprotein of influenza virus A/Victoria/3/75. Journal of Virology. American
933 Society for Microbiology (ASM); 1996 Jun;70(6):3385–91.

934 50. Hutchinson EC, Denham EM, Thomas B, Trudgian DC, Hester SS, Ridlova G, et al.
935 Mapping the phosphoproteome of influenza A and B viruses by mass spectrometry.
936 Gack MU, editor. PLoS Pathog. Public Library of Science; 2012;8(11):e1002993.

937 51. Zheng W, Li J, Wang S, Cao S, Jiang J, Chen C, et al. Phosphorylation Controls the
938 Nuclear-Cytoplasmic Shuttling of Influenza A Virus Nucleoprotein. Lyles DS, editor.

Journal of Virology. American Society for Microbiology Journals; 2015 Jun 1;89(11):5822–34.

52. Han Q, Chang C, Li L, Klenk C, Cheng J, Chen Y, et al. Sumoylation of influenza A virus nucleoprotein is essential for intracellular trafficking and virus growth. J Virol. American Society for Microbiology; 2014 Aug;88(16):9379–90.

53. Bao Y, Bolotov P, Dernovoy D, Kiryutin B, Zaslavsky L, Tatusova T, et al. The influenza virus resource at the National Center for Biotechnology Information. J Virol. American Society for Microbiology Journals; 2008 Jan;82(2):596–601.

54. Drummond AJ, Rambaut A. BEAST: Bayesian evolutionary analysis by sampling trees. BMC evolutionary biology. BioMed Central; 2007 Nov 8;7(1):214.

55. de Wit E, Spronken MIJ, Bestebroer TM, Rimmelzwaan GF, Osterhaus ADME, Fouchier RAM. Efficient generation and growth of influenza virus A/PR/8/34 from eight cDNA fragments. Virus Res. 2004 Jul;103(1-2):155–61.

56. Park H-S, Liu G, Thulasi Raman SN, Landreth SL, Liu Q, Zhou Y. NS1 Protein of 2009 Pandemic Influenza A Virus Inhibits Porcine NLRP3 Inflammasome-Mediated Interleukin-1 Beta Production by Suppressing ASC Ubiquitination. López S, editor. J Virol. American Society for Microbiology Journals; 2018 Apr 15;92(8):55.

57. Carrasco M, Amorim MJ, Digard P. Lipid raft-dependent targeting of the influenza A virus nucleoprotein to the apical plasma membrane. Traffic. 2004 Dec;5(12):979–92.

58. Noton SL, Medcalf E, Fisher D, Mullin AE, Elton D, Digard P. Identification of the domains of the influenza A virus M1 matrix protein required for NP binding, oligomerization and incorporation into virions. J Gen Virol. 2007 Aug;88(Pt 8):2280–90.

59. Amorim MJ, Read EK, Dalton RM, Digard P. Nuclear export of influenza A virus mRNAs requires ongoing RNA polymerase II activity. Traffic. 2007 Jan;8(1):1–11.

60. Hutchinson EC, Curran MD, Read EK, Gog JR, Digard P. Mutational analysis of cis-acting RNA signals in segment 7 of influenza A virus. J Virol. 2008 Dec;82(23):11869–79.

61. Matrosovich M, Matrosovich T, Carr J, Roberts NA, Klenk H-D. Overexpression of the alpha-2,6-sialyltransferase in MDCK cells increases influenza virus sensitivity to neuraminidase inhibitors. Journal of Virology. American Society for Microbiology Journals; 2003 Aug;77(15):8418–25.

62. Gaunt E, Wise HM, Zhang H, Lee LN, Atkinson NJ, Nicol MQ, et al. Elevation of CpG frequencies in influenza A genome attenuates pathogenicity but enhances host response to infection. Elife. eLife Sciences Publications Limited; 2016;5:e12735.

63. Morgan SB, Holzer B, Hemmink JD, Salguero FJ, Schwartz JC, Agatic G, et al. Therapeutic Administration of Broadly Neutralizing FI6 Antibody Reveals Lack of Interaction Between Human IgG1 and Pig Fc Receptors. Front Immunol. Frontiers; 2018;9:865.

64. Halbur PG, Paul PS, Frey ML, Landgraf J, Eernisse K, Meng XJ, et al. Comparison of the pathogenicity of two US porcine reproductive and respiratory syndrome virus isolates with that of the Lelystad virus. Vet Pathol. 1995 Nov;32(6):648–60.

65. Vidaña B, Martínez J, Martínez-Orellana P, García Migura L, Montoya M, Martorell J, et al. Heterogeneous pathological outcomes after experimental pH1N1 influenza infection in ferrets correlate with viral replication and host immune responses in the lung. Vet Res. BioMed Central; 2014;45(1):85.

66. Morgan SB, Hemmink JD, Porter E, Harley R, Shelton H, Aramouni M, et al. Aerosol Delivery of a Candidate Universal Influenza Vaccine Reduces Viral Load in Pigs Challenged with Pandemic H1N1 Virus. J Immunol. American Association of Immunologists; 2016 Jun 15;196(12):5014–23.

67. McHugh ML. Multiple comparison analysis testing in ANOVA. Biochem Med (Zagreb). 2011;21(3):203–9.

Supplementary Information

Table S1. Distribution of NP start codons by major IAV lineage in the stratified subsampled data set.

Host-lineage	Avian	Swine	Human	Other	Total Sequences	Conventional Start %	uAUG Start %
Avian-Americas	2642	2	2	5	2651	99.9	0.1
Avian-Eurasia	1449	22	56	46	1573	99.6	0.4
Equine-Canine	0	2	0	71	73	100.0	0.0
Human-pdm2009	2	6	232	0	240	2.1	97.9
Human-Seasonal	1	28	894	1	924	99.6	0.4
Swine-Classical-Triple	15	352	23	0	390	8.7	91.3
Swine-Eurasia	1	68	4	0	73	94.5	5.5
Variant-pdm2009	2	122	181	4	309	7.8	92.2
Unclassified	2	1	0	6	9	100.0	0.0

In the stratified subsampled data set of 6242 segment 5 sequences, the distribution of NP start codons by host was similar to that in the full data set, although the percentage of sequences with an upstream start codon was somewhat reduced compared to the full data set (see Table 1).

Table S2. (see separate Excel file). Stratified subsampled dataset of IAV segment 5 sequences, classified according to the presence (TRUE) or absence (FALSE) of an in-frame upstream AUG codon in the NP gene, as well as H and N subtype, continent, region and country of isolation, host and date of isolation and named clade. The position of the first AUG codon in the segment (first_start) and the identity of the nucleotide triplet at the location of the uAUG (upstream3) are also tabulated.

1009

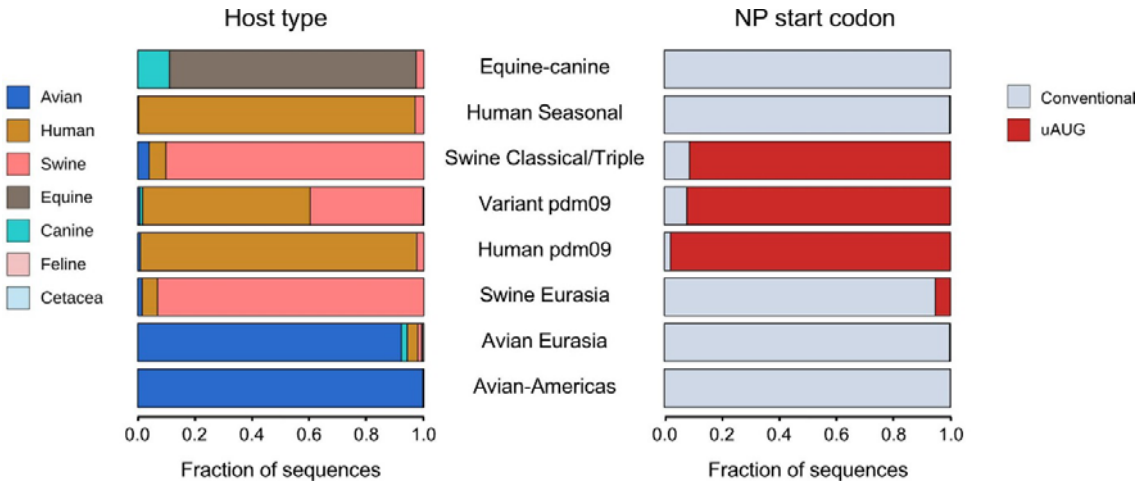

1010

1011 **Figure S1.** Distribution of hosts and segment 5 start codon positions by major IAV lineage in
1012 the stratified subsampled data set.

1013

1014

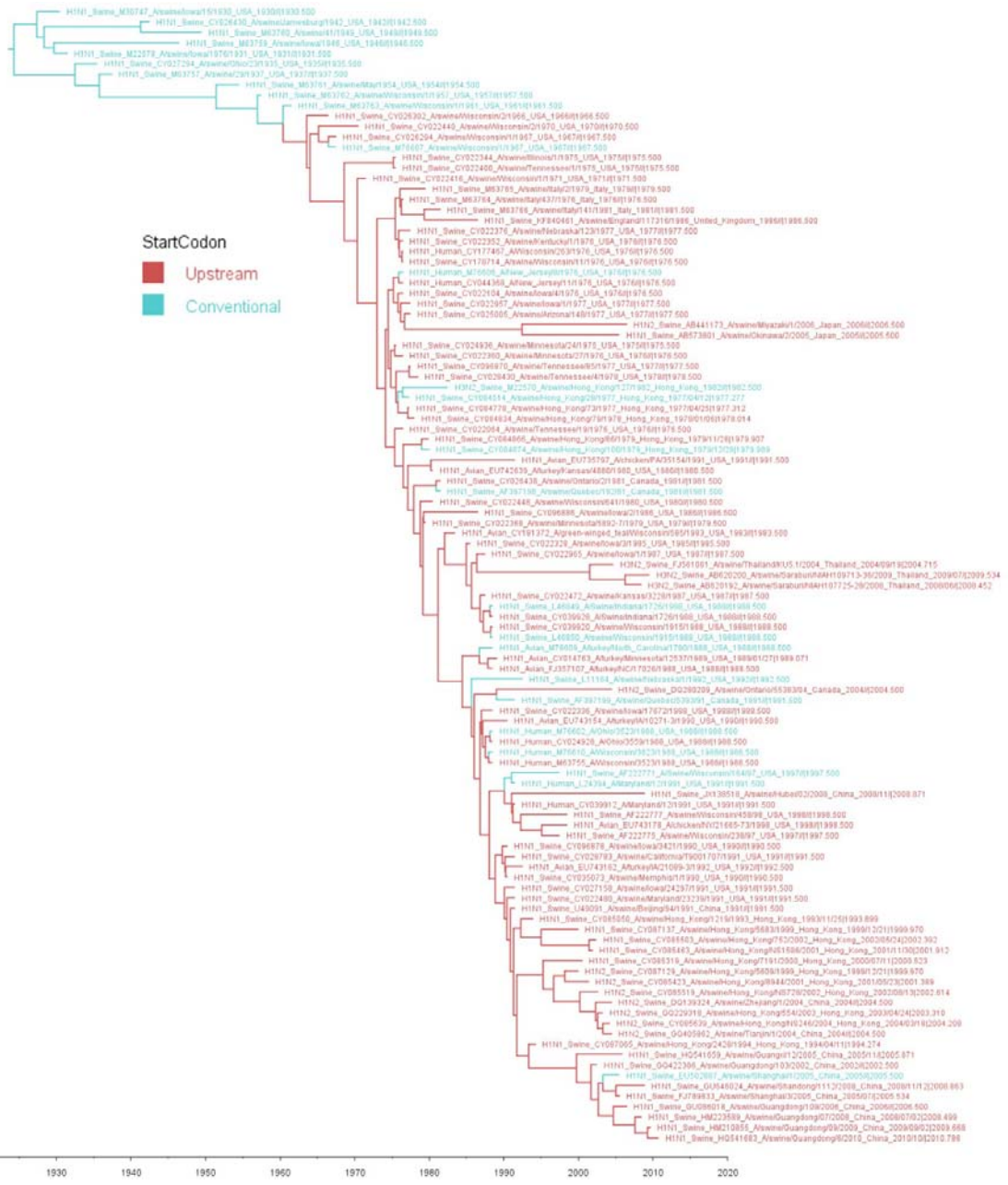

Figure S2. Time scaled tree of segment 5 from the classical swine virus clade with skygrid tree prior and NP start codon as a discrete trait. Sequences in red possess the uAUG, those in blue do not. The uAUG codon first appeared at an estimated date in 1962 (range 1958-1965) in H1N1 swine IAV in Wisconsin. This is based on the mutation happening somewhere on the branch between nodes 1960.41 [Highest Posterior Density (HPD): 1958.1 - 1961.5] and 1963.55 [HPD: 1961.2 - 1965.7]).

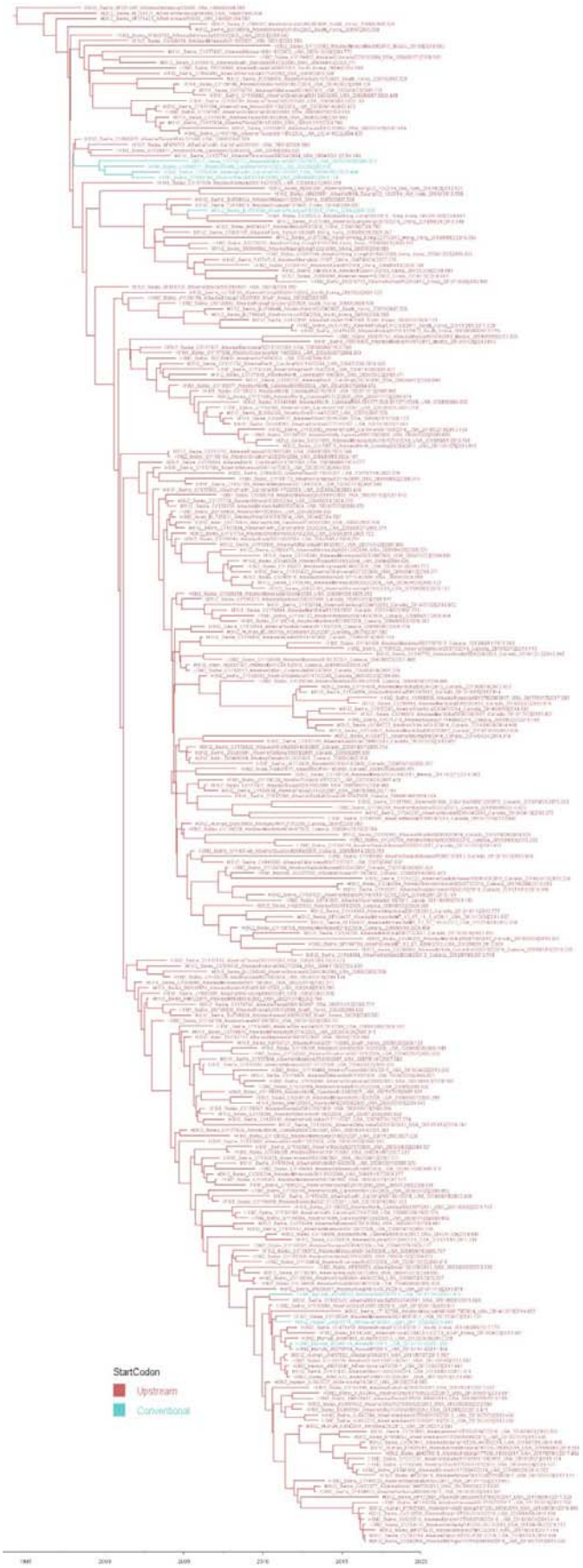

Figure S3. Time scaled tree of segment 5 from the triple reassortant swine virus clade with skygrid tree prior and NP start codon as a discrete trait. Sequences in red possess the uAUG, those in blue do not. Triple reassortant viruses most likely inherited an uAUG-containing segment 5 from their classical swine progenitor and subsequently, have largely kept it.

Strain	Accession	Host	Subtype	Country
A/duck/New_York/16873/1999	CY014891	Avian	H6N2	USA
A/mallard/Maryland/887/2002	EU026010	Avian	H6N1	USA
A/chicken/Italy/322/2001	CY021552	Avian	H7N1	Italy
A/chicken/Israel/702/2008	GQ148843	Avian	H9N2	Israel
A/duck/Taiwan/DC167/2010	KC693624	Avian	H1N3	Taiwan
A/Albany/20/1974	CY021096	Human	H3N2	USA
A/Bilthoven/2271/1976	KC296468	Human	H3N2	Netherlands
A/Singapore/64K/2007	KP223188	Human	H3N2	Singapore
A/Victoria/600/2016	CY254980	Human	H3N2	Australia

Table S3. Sporadic occurrences of the uAUG in avian and human seasonal viruses. Isolate name, subtype, segment 5 sequence accession code, host and country of isolation are tabulated. Most isolates are too temporally and/or geographically separate to represent linked events; the H6 duck isolates from the eastern USA in 1999 and 2002 and the human H3N2 isolates from the mid 1970s might be exceptions.

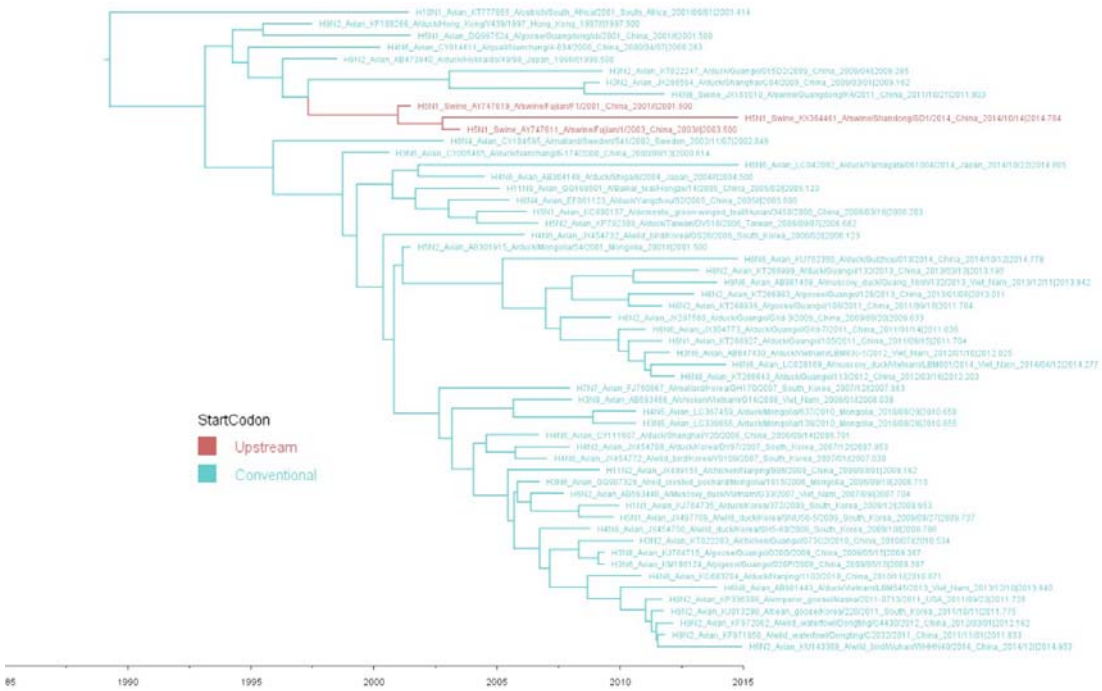

Figure S4. Acquisition of the segment 5 uAUG codon associated with epizootic transfer from ducks to swine. A time scaled tree of segment 5 from an avian virus clade with skygrid tree prior and NP start codon as a discrete trait. Sequences in red possess the uAUG, those in blue do not. The 5'-UTR sequence of segment 5 from the closest relative of the uAUG-possessing A/swine/Fujian/2001 and /2003 viruses (A/duck/Zhejiang/11/2000(H5N1)) has not been reported, making it uncertain whether the polymorphism occurred before or after the host-range jump. Note also that the apparent persistence of the uAUG-containing swine virus in China until 2014 may be an artefact, as all eight segments of A/swine/Shandong/SD1/2014 have the corresponding genes from A/swine/Fujian viruses from the early 2000s as their closest relatives (> 99.7% nucleotide identity) and conversely, lack close relatives from the 2010s, raising the possibility of laboratory contamination.

Figure S5. Acquisition of the segment 5 uAUG codon within the Eurasian swine IAV lineage. A time scaled tree of segment 5 from an avian virus clade with skygrid tree prior and NP start codon as a discrete trait. Sequences in red possess the uAUG, those in blue do not.

Table S4. Summary statistics for minireplicon assay curve fitting data reported in Figures 3C, D. See separate Excel file.

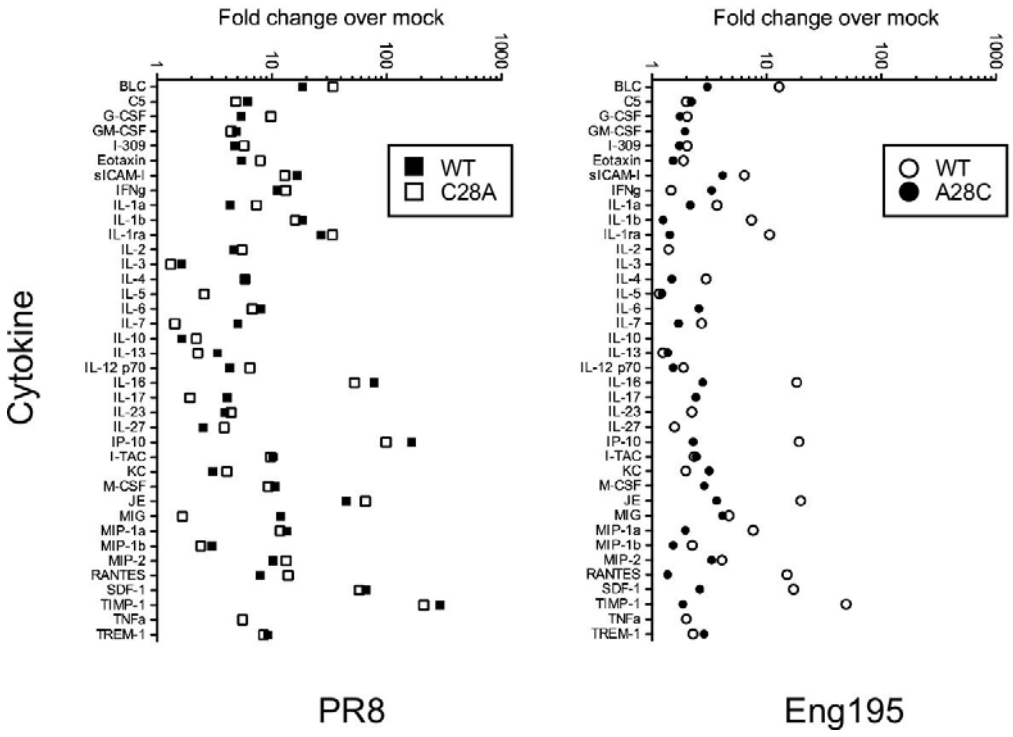

Figure S6. Cytokine levels in infected mouse lung. Lung homogenates from mice infected with the indicated viruses or mock infected animals were pooled and the levels of various cytokines measured by cytokine array.

Table S5. (see separate Excel file). Formalin-fixed lung sections were stained with haematoxylin and eosin and examined by a veterinary pathologist. Six pathological changes (epithelial cell degeneration and necrosis, perivascular inflammation, peribronchial inflammation, interstitial inflammation, interstitial necrosis and lymphocyte cuffing) were scored on a scale of 0-4. The percentage of lung affected was estimated visually. The pathological changes present along with a consideration of the area of lung affected was used to give an overall qualitative score of the severity of histopathological changes. Slides from three mice (22, 14 and 9) were not scored and excluded from the analysis due to marked atelectasis (artefact) which precluded assessment of pathological changes.

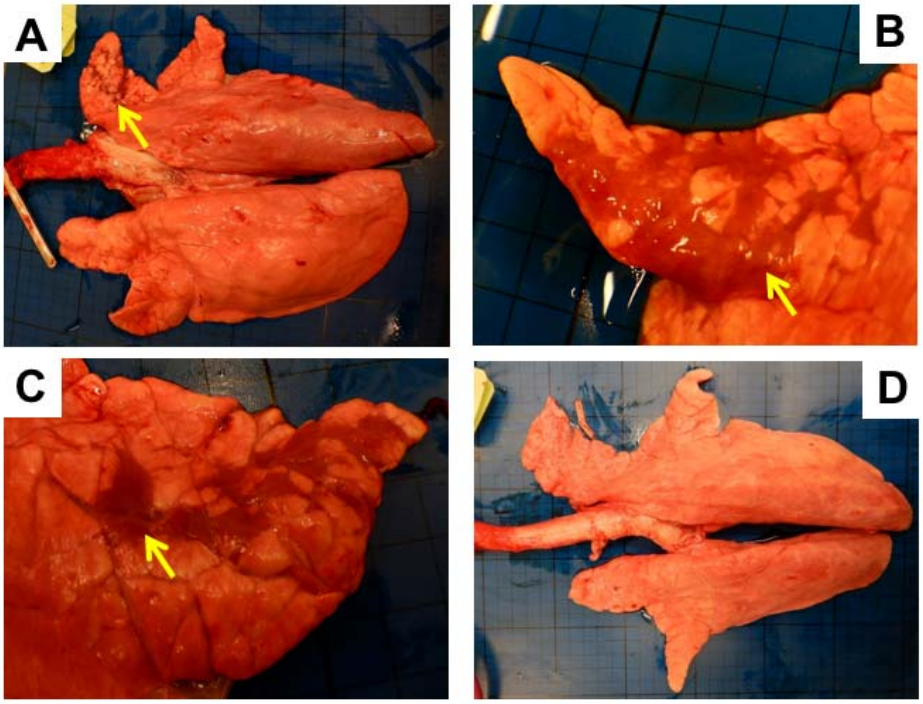

Figure S7. Macroscopic pathology of pig lungs 4 days post challenge with WT (A, B and C) and A28C Eng195 (D) viruses. Arrows indicate areas of atelectasis observed in the apical lobe of the right lung (A) and medial lobes (B and C). Some animals from the A28C group exhibited no remarkable gross pathology (D).

Table S6. (see separate Excel file). Histopathological changes in the stained lung tissue sections were scored by a veterinary pathologist blinded to the treatment group. Lung histopathology was scored using five parameters (necrosis of the bronchiolar epithelium, airway inflammation, perivascular/bronchiolar cuffing, alveolar exudates and septal inflammation) scored on a five-point scale of 0 to 4 and then summed to give a total slide score ranging from 0 to 20 and a total animal score from 0 to 100 (63). The Iowa system includes both histological lesions and immunohistochemical staining for NP (35).